

# Spectral Subspace Clustering for Attributed Graphs

Xiaoyang Lin  
Hong Kong Baptist University  
csxylin@hkbu.edu.hk

Haoran Zheng  
Hong Kong Baptist University  
cshrzhen@hkbu.edu.hk

Renchi Yang  
Hong Kong Baptist University  
renchi@hkbu.edu.hk

Xiangyu Ke  
Zhejiang University  
xiangyu.ke@zju.edu.cn

## ABSTRACT

Subspace clustering seeks to identify subspaces that segment a set of  $n$  data points into  $k$  ( $k \ll n$ ) groups, which has emerged as a powerful tool for analyzing data from various domains, especially images and videos. Recently, several studies have demonstrated the great potential of subspace clustering models for partitioning vertices in attributed graphs, referred to as SCAG. However, these works either demand significant computational overhead for constructing the  $n \times n$  self-expressive matrix, or fail to incorporate graph topology and attribute data into the subspace clustering framework effectively, and thus, compromise result quality.

Motivated by this, this paper presents two effective and efficient algorithms,  $S^2CAG$  and  $M-S^2CAG$ , for SCAG computation. Particularly,  $S^2CAG$  obtains superb performance through three major contributions. First, we formulate a new objective function for SCAG with a refined representation model for vertices and two non-trivial constraints. On top of that, an efficient linear-time optimization solver is developed based on our theoretically grounded problem transformation and well-thought-out adaptive strategy. We then conduct an in-depth analysis to disclose the theoretical connection of  $S^2CAG$  to conductance minimization, which further inspires the design of  $M-S^2CAG$  that maximizes the modularity. Our extensive experiments, comparing  $S^2CAG$  and  $M-S^2CAG$  against 17 competitors over 8 benchmark datasets, exhibit that our solutions outperform all baselines in terms of clustering quality measured against the ground truth while delivering high efficiency.

## CCS CONCEPTS

• **Computing methodologies** → **Cluster analysis; Spectral methods**; • **Information systems** → **Clustering**.

## KEYWORDS

attributed graph, subspace clustering, conductance, modularity

### ACM Reference Format:

Xiaoyang Lin, Renchi Yang, Haoran Zheng, and Xiangyu Ke. 2025. Spectral Subspace Clustering for Attributed Graphs. In *Proceedings of the 31th ACM SIGKDD Conference on Knowledge Discovery and Data Mining (KDD '25)*.

Permission to make digital or hard copies of part or all of this work for personal or classroom use is granted without fee provided that copies are not made or distributed for profit or commercial advantage and that copies bear this notice and the full citation on the first page. Copyrights for third-party components of this work must be honored. For all other uses, contact the owner/author(s).

KDD '25, August 3–7, 2025, Toronto, Canada

© 2025 Copyright held by the owner/author(s).

ACM ISBN 978-1-4503-XXXX-X/18/06.

<https://doi.org/XXXXXXXX.XXXXXXX>

August 3–7, 2025, Toronto, Canada. ACM, New York, NY, USA, 15 pages.  
<https://doi.org/XXXXXXXX.XXXXXXX>

## 1 INTRODUCTION

*Attributed graphs* are an omnipresent data structure used to model the interplay between entities characterized by rich attributes, such as social networks, citation graphs, World Wide Web, and transportation grids. Clustering such graphs, i.e., partition vertices therein into disjoint groups, has gained massive attention over the past decade [7, 14, 56], due to its encouraging performance by leveraging the complementary nature of graph topology and attributes, as well as its extensive use in community detection [51, 83], Bioinformatics [8, 12], anomaly identification [61], online advertising and recommendation [20, 50], etc.

This problem remains tenaciously challenging as it requires joint modeling of graph structures and nodal attributes that present heterogeneity, complex semantics, and noises. State-of-the-art solutions [18, 44] are built upon deep learning techniques, especially *graph convolutional neural networks* [43], which first aggregates attributes of neighbors in the graph before mapping attribute vectors to low-dimensional feature representations of vertices for clustering. Notwithstanding promising results reported, these works rely on a strong assumption that neighboring vertices should have high attribute homogeneity, rendering them vulnerable to attributed networks contaminated with irrelevant and noisy data [109]. In addition, this category of methods suffers from poor scalability and demands tremendous computational resources for model training, especially on large graphs.

*Subspace clustering* (SC) [86] is a fundamental technique in data mining used for analyzing high-dimensional data including images, text, gene expression data, and so on [22]. Intrinsically, it simultaneously clusters the data into multiple subspaces and identifies a low-dimensional subspace fitting each group of points, thereby eradicating the adverse impacts of irrelevant and noisy dimensions (i.e., features) [71]. More precisely, the linchpin of SC is to construct a *self-expressive matrix* (SEM) that models the affinity of all data points such that each data point can be written as a linear combination of others. Subsequent research [29, 102] further bolsters the SC performance by working in tandem with *multi-view data* where the data set is represented by multiple distinct feature sets.

Inspired by its success, in recent years, several attempts [28, 46, 63] have been made towards extending the principle of SC to attributed graphs for enhanced clustering quality, given that an attributed graph embodies two sets of features (i.e., structures and attributes). For simplicity, we refer to this line of research as SCAG (short for subspace clustering for attributed graphs) henceforth. Among these

works, SAGSC [28] heavily relies on feature augmentation via polynomial combinations of the extracted features. Such hand-crafted features decrease the model interpretability and its generalization to diverse datasets and engender suboptimal result quality. Ma et al. [63] and Li et al. [46] directly construct the SEM, resulting in space and computation costs quadratic in the number of vertices. As an aftermath, they struggle to cope with real attributed graphs, which often encompass numerous vertices, edges, and a sheer volume of attribute data. Furthermore, despite their empirical effectiveness on attributed graphs, there is little theoretical interpretation and analysis of these SCAG approaches.

To overcome the deficiencies of existing solutions, this paper presents  $S^2CAG$  and  $M-S^2CAG$  which offer superb clustering performance while being efficient, through a series of novel algorithmic designs and rigorous theoretical analyses. First and foremost,  $S^2CAG$  formulates the optimization objective of SCAG based on our *normalized smoothed representations* (NSR) for vertices with a *low-rank constraint* [52] and an orthogonality regularization. Particularly, NSR enables stronger representation capacity by augmenting *graph Laplacian smoothing*-based vertex representations [19] with normalized topology, attribute matrices, and weights. The two additional constraints improve the resulting SEM’s robustness to noises and outliers, and meanwhile, facilitate the design of our efficient optimization solvers. Taking inspiration from the *orthogonal Procruste problem* [77],  $S^2CAG$  transforms the problem into a simple truncated *singular value decomposition* (SVD) [32] without materializing the SEM, whereby we devise adaptive solvers that merely involve efficient operations on tall-and-skinny matrices. Moreover, we conduct detailed theoretical analyses digesting  $S^2CAG$ ’s relation to graph clustering that optimizes *conductance* [57]. This finding further guides us to upgrade  $S^2CAG$  to  $M-S^2CAG$  which essentially maximizes *modularity* [69] on affinity graphs for clustering.

Our empirical studies, which evaluate  $S^2CAG$  and  $M-S^2CAG$  against 17 baselines over 8 real-life attributed graphs with ground-truth clusters, showcase the consistent superiority of our solutions in terms of result quality and efficiency. On the *ArXiv* dataset with 169K vertices and 1.3M edges,  $M-S^2CAG$  advances the state of the art by a significant improvement of 2.2% in clustering accuracy without degrading the practical efficiency.

## 2 RELATED WORK

### 2.1 Subspace Clustering

Foundational subspace clustering algorithms like Sparse Subspace Clustering (SSC) [21], Low-Rank Representation (LRR) [52], and Multiple Subspace Representation (MSR) [60] focus on learning an affinity matrix, which is then employed in spectral clustering to discern underlying data structures.

However, the traditional methods often grapple with high computational complexity. In response, a suite of low-rank sparse methods has been proposed [10, 13, 24, 58], which simultaneously reduce computational load and improve algorithmic efficiency and scalability. Further enhancements in subspace clustering algorithms have been achieved through methods that emphasize local structure-preserving and kernel techniques [40, 53, 59, 72]. For an in-depth exploration, we kindly refer to surveys [41, 74, 86]. Furthermore, a number of studies have successfully incorporated deep learning into

the traditional subspace clustering paradigm [9, 39, 73, 105, 106]. These approaches leverage end-to-end training to learn proximities in latent subspaces, ultimately producing a representative coefficient matrix that is critical for subsequent clustering processes.

### 2.2 Attributed Graph Clustering

Extensive studies have identified various methods for addressing attribute graph clustering (AGC) challenges. These include approaches grounded in edge-weight-based [15, 66, 68, 75, 81], distance-based [23, 67, 108] and probabilistic-model-based methods [70, 93, 99, 101]. For detailed insights, readers could refer to related reviews [7, 14, 47, 97].

Recently, common practice involves integrating structural connectivity into vertex attributes to derive vertex embeddings [1, 16, 48, 96, 108], which are then used to perform clustering via established techniques such as KMeans. Lai et al. [44] conducted a comprehensive assessment of all existing deep attribute graph clustering (DAGC) methods [5, 17, 33, 37, 55, 85] for AGC, which capture both the topological and attribute information of graphs, integrating this fused information to facilitate the learning of vertex embeddings. To augment the proficiency of vertex representation learning, certain models embedded in the DAGC framework have embraced graph attention mechanisms [88, 91, 104, 107], coupled with advanced graph contrastive learning methodologies [34, 100, 103]. Beyond the enhancement of vertex representations to achieve superior clustering performance, certain models [27, 54, 64] incorporate the outcomes of vertex clustering into deep learning frameworks to optimize the cluster distribution.

Owing to the high efficiency demonstrated by subspace clustering algorithms, a growing body of research [31, 46, 63, 90] has been applying these algorithms to AGC. These methodologies perform SC algorithms on graphs that integrate both topological and attribute information. Among these, SAGSC [28] stands out as a state-of-the-art algorithm, characterized by its scalability and efficiency in SC. Nevertheless, the previously mentioned methodologies are constrained by their incapacity to thoroughly exploit the graph’s topological framework and nodal attribute data, concomitant with an absence of low-complexity SC underpinned by stringent mathematical principles.

## 3 PROBLEM FORMULATION

### 3.1 Notations and Terminology

Throughout this paper, sets are symbolized by calligraphic letters, e.g.,  $\mathcal{V}$ . Matrices (resp. vectors) are denoted as bold uppercase (resp. lowercase) letters, e.g.,  $\mathbf{X}$  (resp.  $\mathbf{x}$ ). The transpose and inverse of matrix  $\mathbf{X}$  are denoted by  $\mathbf{X}^\top$  and  $\mathbf{X}^{-1}$ , respectively. The  $i$ -th row (resp. column) of  $\mathbf{X}$  is represented by  $\mathbf{X}_i$  (resp.  $\mathbf{X}_{\cdot,i}$ ). Accordingly,  $X_{i,j}$  stands for the  $(i, j)$ -th entry of  $\mathbf{X}$ .  $\|\mathbf{X}\|_F$  stands for the Frobenius norm of matrix  $\mathbf{X}$ . We use  $\mathbf{I}$  to denote the identity matrix and its size is obvious from context. We refer to the left (resp. right) singular vectors of  $\mathbf{X}$  that correspond to its  $k$ -largest singular values as *top- $k$  left (resp. right) singular vectors*. The  $k$  eigenvectors of  $\mathbf{X}$  corresponding to its  $k$  largest eigenvalue in absolute value are referred to as the  *$k$ -largest eigenvectors of  $\mathbf{X}$* .

An *attributed graph* is defined as  $\mathcal{G} = (\mathcal{V}, \mathcal{E}, \mathbf{X})$ , composed of a set  $\mathcal{V} = \{v_1, v_2, \dots, v_n\}$  of  $n$  vertices (a.k.a. nodes), a set  $\mathcal{E} \subseteq \mathcal{V} \times \mathcal{V}$

of  $m$  edges, and an  $n \times d$  attribute matrix  $X$ . Each vertex  $v_i \in \mathcal{V}$  is characterized by a length- $d$  attribute vector  $X_i$  and each edge  $(v_i, v_j) \in \mathcal{E}$  connects two vertices  $v_i, v_j \in \mathcal{V}$ . For each vertex  $v_i$ , we denote by  $\mathcal{N}_{v_i} = \{v_j \in \mathcal{V} | (v_i, v_j) \in \mathcal{E}\}$  the set of direct neighbors of  $v_i$ , and by  $d(v_i) := |\mathcal{N}_{v_i}|$  the degree of  $v_i$ . We use  $A \in \{0, 1\}^{n \times n}$  to represent the adjacency matrix (with self-loops) of  $\mathcal{G}$ , where  $A_{i,j} = 1$  if  $(v_i, v_j) \in \mathcal{E}$  or  $v_i = v_j$ , and 0 otherwise. In this paper, we consider undirected graphs, and hence,  $A$  is symmetric. The diagonal degree matrix of  $\mathcal{G}$  is symbolized by  $D$ , wherein the diagonal entry  $D_{i,i} = d(v_i) + 1$ . The normalized adjacency matrix  $\hat{A}$  and transition matrix  $P$  of  $\mathcal{G}$  are defined as  $D^{-\frac{1}{2}}AD^{-\frac{1}{2}}$  and  $D^{-1}A$ , respectively. In particular,  $P_{i,j}^t$  denotes the probability that a  $t$ -hop simple random walk from vertex  $v_i$  would stop at vertex  $v_j$ . Accordingly, the *personalized PageRank* (PPR) [38] of vertex  $v_j$  w.r.t. vertex  $v_i$  over  $\mathcal{G}$  is defined as  $\pi_{v_i}(v_j) = \sum_{t=0}^{\infty} (1 - \alpha)\alpha^t P_{i,j}^t$ , where  $\alpha$  stands for the decay factor.

### 3.2 Graph Laplacian Smoothing

Given a graph  $\mathcal{G}$  and a signal vector  $\mathbf{x} \in \mathbb{R}^n$ , the goal of *graph Laplacian smoothing* [19] is to find a smoothed version of  $\mathbf{x}$ , i.e.,  $\bar{\mathbf{x}} \in \mathbb{R}^n$ , such that the following objective is optimized:

$$\min_{\bar{\mathbf{x}}} \|\bar{\mathbf{x}} - \mathbf{x}\|_2^2 + \alpha \cdot \bar{\mathbf{x}}^\top L \bar{\mathbf{x}}, \quad (1)$$

where  $L = I - \hat{A}$  denotes the normalized Laplacian matrix of  $\mathcal{G}$  and  $\alpha \in (0, 1)$  is the parameter balancing two terms. If we consider  $d$  different signal vectors, e.g., the attribute matrix  $X \in \mathbb{R}^{n \times d}$ , the overall optimization objective is therefore

$$\min_{\bar{X}} (1 - \alpha) \cdot \|\bar{X} - X\|_F^2 + \alpha \cdot \text{trace}(\bar{X}^\top L \bar{X}), \quad (2)$$

The first term in Eq. (2) seeks to reduce the discrepancy between the input matrix  $X$  and its smoothed version  $\bar{X}$ . By [87],  $\text{trace}(\bar{X}^\top L \bar{X})$  can be rewritten as  $\sum_{(v_i, v_j) \in \mathcal{E}} \left\| \frac{\bar{X}_i}{\sqrt{d(v_i)}} - \frac{\bar{X}_j}{\sqrt{d(v_j)}} \right\|_2^2$ , meaning that the second term enforces the smoothed attribute vectors  $\bar{X}_i, \bar{X}_j$  of any adjacent vertices  $(v_i, v_j) \in \mathcal{E}$  to be similar.

**LEMMA 3.1 (NEUMANN SERIES [35]).** *If the eigenvalue  $\lambda_i$  of  $M \in \mathbb{R}^{n \times n}$  satisfies  $|\lambda_i| < 1 \forall 1 \leq i \leq n$ , then  $(I - M)^{-1} = \sum_{t=0}^{\infty} M^t$ .*

As demystified in recent studies [62, 110], after removing non-linear operations, graph convolutional layers in popular *graph neural network* (GNN) models, e.g., APPNP [30], GCNII [11], essentially optimize the objective in Eq. (2) and the closed-form solution (i.e., final vertex representations) can be represented as

$$\bar{X} = (1 - \alpha) \cdot ((1 - \alpha) \cdot I + \alpha \cdot L)^{-1} X = \sum_{t=0}^{\infty} (1 - \alpha)\alpha^t \hat{A}^t X \quad (3)$$

by taking the derivative of Eq. (2) with respect to  $\bar{X}$  to zero and applying Lemma 3.1 with  $M = \alpha \cdot \hat{A}$  ( $\alpha \in (0, 1)$ ). Since  $\hat{A}^t = D^{\frac{1}{2}} P^t D^{-\frac{1}{2}}$ , we can rewrite  $\sum_{t=0}^{\infty} \alpha^t \hat{A}^t$  as  $D^{\frac{1}{2}} \cdot (\sum_{t=0}^{\infty} \alpha^t P^t) \cdot D^{-\frac{1}{2}}$ . As such, the smoothed representation  $\bar{X}_i$  of each vertex  $v_i \in \mathcal{V}$  obtained in Eq. (3) is a summation of the attribute vectors of all vertices weighted by their degree-reweighted PPR w.r.t.  $v_i$ , i.e.,

$$\bar{X}_i = \sum_{v_j \in \mathcal{V}} \sqrt{\frac{d(v_j)}{d(v_i)}} \cdot \pi_{v_i}(v_j) \cdot X_j. \quad (4)$$

In practice,  $\bar{X}$  in Eq. (3) is usually approximated via a  $T$ -order truncated version  $\sum_{t=0}^T (1 - \alpha)\alpha^t \hat{A}^t X$ , where  $T$  is typically dozens.

### 3.3 Subspace Clustering

Let  $F \in \mathbb{R}^{n \times d}$  be a data matrix for  $n$  distinct data samples where each data sample  $i \in \{1, 2, \dots, n\}$  is represented by a  $d$ -dimensional feature vector  $F_i$ . *Subspace clustering* aims to group data samples into  $k$  disjoint clusters  $\{C_1, C_2, \dots, C_k\}$ , which is based on the assumption that data samples lie in a union of subspaces [86]. *Self-Expression Model* [58] is the most widely adopted objective formulation for subspace clustering. In this model, each data sample is assumed to be expressed as a linear combination of other data samples in the same subspace:

$$\min_{S \in \mathbb{R}^{n \times n}} \|F - SF\|_F^2 + \Omega(S), \quad (5)$$

where  $S \in \mathbb{R}^{n \times n}$  is known as the *self-expressive matrix* (SEM) (a.k.a. *coefficient matrix*). The first term is to reconstruct  $F$  via  $S$  and  $F$ , while the regularization term  $\Omega(S)$  is introduced to impose constraints rendering  $S$  meet certain structures or averting trivial solutions, e.g.,  $I$ . Popular constraints include *sparsity constraint* [89] and *low-rank representation* (LRR) [52]. The former minimizes the vector  $L_1$  norm of  $S$  to induce sparsity, whereas LRR minimizes the rank of  $S$  such that  $S$  captures the global correlation of the data samples [82]. In simpler terms, with the low-rank constraint, correlations between data samples are strengthened within clusters but weakened across clusters. Besides, by virtue of the low-rank setting, we can extract dominant patterns/features in the data while filtering out minor deviations, and hence, improve the robustness to noise and outliers. The resulting SEM  $S$  is then used to form an affinity matrix  $\frac{S+S^\top}{2}$  that quantifies the affinity of every two data samples. Based thereon, *spectral clustering* [87] can be applied to the affinity matrix for clustering.

### 3.4 Subspace Clustering for Attributed Graphs

To extend subspace clustering to attributed graphs, a simple and straightforward idea is to employ the vertex representations  $\bar{X}$  obtained via GLS in Eq. (3) as the data feature matrix  $F$ .

**Normalized Smoothed Representations.** We argue that the direct adoption of  $\bar{X}$  for subspace clustering is problematic. First,  $\alpha$  in  $\bar{X}$  (Eq. (3)) is restricted within the range  $(0, 1)$  to avoid negative or zero values due to the existence of  $1 - \alpha$ . Although  $1 - \alpha$  can be removed, we still cannot assign large values to  $\alpha$  as it leads to weighty coefficients  $\alpha^t$  that might overwhelm the entries in  $\hat{A}^t$  and other terms. Thereby,  $\alpha^t$  is constrained to monotonically decrease as  $t$  increases, limiting the capacity of  $\bar{X}$  in capturing the topological semantics in various graphs. Moreover, each entry  $\hat{A}_{i,j} \forall v_i, v_j \in \mathcal{V}$  merely considers the degrees of endpoints  $v_i$  and  $v_j$  and overlooks the structures of other adjacent vertices of  $v_i$  or  $v_j$ , which is apt to cause biased attribute aggregation in Eq. (4). Similar issues arise on  $X$ , where attribute vectors of vertices fall on different scales. In response, we propose to calculate the *normalized smoothed representations* (NSR) of vertices in  $\mathcal{G}$  as  $F$  via

$$Z = \sum_{t=0}^T \frac{\alpha^t}{\sum_{t=0}^T \alpha^t} \hat{P}^t \hat{X} = \sum_{t=0}^T \frac{(1-\alpha)\alpha^t}{1-\alpha^{T+1}} \hat{P}^t \hat{X}, \quad (6)$$

where an  $L_1$  normalization is applied to all weights  $1, \alpha, \dots, \alpha^T$  such that  $\alpha$  is allowed to exceed 1. As for  $\hat{A}$  and  $X$  in Eq. (3), we

substitute them by their normalized versions  $\hat{P}$  and  $\hat{X}$  defined by

$$\hat{P}_{i,j} = \frac{\hat{A}_{i,j}}{\sum_{v_\ell \in \mathcal{V}} \hat{A}_{i,\ell}} \quad \forall v_i, v_j \in \mathcal{V} \quad \text{and} \quad \hat{X}_i = \frac{X_i}{\sqrt{\sum_{v_j \in \mathcal{V}} X_i \cdot X_j^\top}} \quad \forall v_i \in \mathcal{V}.$$

**Objective Function.** Based on NSR  $Z$  and Eq. (5), we impose the *low-rank constraint* (i.e., LRR) and *soft orthogonality regularization* to SEM  $S$  and formulate the main objective function for SCAG as

$$\min_{S \in \mathbb{R}^{n \times n}} \|Z - SZ\|_F^2 + \|S\|_* + \|S^\top S - I\|_F^2, \quad (7)$$

where the nuclear norm [26]  $\|S\|_*$  is an approximation of  $\text{rank}(S)$  and the regularizer  $\|S^\top S - I\|_F^2$  is introduced to prevent *overcorrelation* between vertices.

The above objective poses two formidable technical challenges. First and foremost, the resulting SEM  $S$  is a dense matrix whose materialization consumes  $O(n^2)$  space storage, which is prohibitive for large graphs. Using such a dense matrix for the rear-mounted spectral clustering further yields an exorbitant expense of  $O(n^2k)$  time. On top of that, the complex constraints and objectives in Eq. (7) lead to numerous iterations till convergence towards its optimization, each of which takes a quadratic time of  $O(n^2)$  due to the high density of  $S$ .

## 4 S<sup>2</sup>CAG APPROACH

To cope with the above-said issues, this section presents a practical algorithm S<sup>2</sup>CAG for SCAG that runs in time linear to the size of  $\mathcal{G}$ . Section 4.1 transforms our optimization objective in Eq. (7) into a simple truncated SVD of  $Z$  based on a rigorous theoretical analysis. Section 4.2 delineates how S<sup>2</sup>CAG implements the SVD and clustering in an adaptive fashion for higher efficiency. In Section 4.3, we establish the theoretical connections between S<sup>2</sup>CAG and minimizing the *conductance* [57] of clusters.

### 4.1 High-level Idea

Note that the ultimate goal of SCAG is to partition  $\mathcal{V}$  into  $k$  disjoint clusters rather than computing the intermediate  $S$ . In light of this, we capitalize on the following theoretical analyses to bypass the explicit construction of  $S$  and streamline the SCAG computation.

**Orthogonal Procrustes Transformation.** Instead of optimizing Eq. (7) directly, we resort to an approximate solution by relaxing its constraints as follows. First of all, recall that minimizing the nuclear norm  $\|S\|_*$  is to reduce the rank of  $S$  as much as possible. However, the spectral clustering stage in SCAG requires computing the  $k$  eigenvectors that correspond to the largest *non-zero* eigenvalues of  $S$  or its Laplacian for clustering. Intuitively, an SEM  $S$  with a rank  $r < k$  has solely  $r$  non-zero eigenvalues, which is incompetent for producing  $k$  meaningful clusters. Simply, we enforce the rank of  $S$  to be  $k$  as a trade-off. With Lemma 4.1<sup>1</sup>, our optimization objective in Eq. (7) is transformed into an *orthogonal Procrustes problem* [77] with a  $k$ -rank constraint over  $S$  by letting  $M = N = Z$  and  $\Omega = S$ .

LEMMA 4.1. *Given matrices  $M$  and  $N$ , the orthogonal Procrustes problem with a  $k$ -rank constraint aims to find matrix  $\Omega$  such that*

$$\min_{\Omega} \|\Omega M - N\|_F^2 + \|\Omega^\top \Omega - I\|_F^2 \text{ s.t. } \text{rank}(\Omega) = k.$$

<sup>1</sup>All proofs can be found in Appendix C.

*The optimal value of  $\Omega$  is  $U^{(k)}V^{(k)\top}$ , where the columns in  $U^{(k)}$  and  $V^{(k)}$  are the top- $k$  left and right singular vectors of  $NM^\top$ , respectively.*

Consequently, an approximate minimizer  $S$  to Eq. (7) is  $U^{(k)}V^{(k)\top}$ , where the columns of  $U^{(k)}$  and  $V^{(k)}$  are the top- $k$  left and right singular vectors of  $ZZ^\top$ , respectively.

LEMMA 4.2.  *$U^{(k)} = V^{(k)}$  and their columns correspond to the top- $k$  left singular vectors of  $Z$ .*

Further, our careful analysis in Lemma 4.2 reveals that SEM  $S = U^{(k)}U^{(k)\top}$ , where  $U^{(k)}$  denotes the top- $k$  left singular vectors of  $Z$ . In turn, the problem in Eq. (7) is reformulated as a simple  $k$ -truncated SVD of  $Z$ .

**Decomposed Spectral Clustering.** Recall that the second step of SCAG is to apply the spectral clustering to the affinity matrix  $\frac{S+S^\top}{2}$ , which first finds the  $k$ -largest eigenvectors  $Y \in \mathbb{R}^{n \times k}$  of affinity matrix  $\frac{S+S^\top}{2}$ , followed by a  $k$ -Means or rounding algorithms [49, 79, 95] over  $Y$  to recast it into a vertex-cluster assignment (VCA) matrix  $C \in \mathbb{R}^{n \times k}$  (corresponding to the clusters  $\{C_1, C_2, \dots, C_k\}$ ):

$$C_{i,j} = \begin{cases} \frac{1}{\sqrt{|C_j|}} & \text{if } v_i \in C_j, \\ 0 & \text{Otherwise.} \end{cases} \quad (8)$$

Given that  $S = U^{(k)}U^{(k)\top}$  is a symmetric matrix, the affinity matrix  $\frac{S+S^\top}{2}$  can be simplified as  $S = U^{(k)}U^{(k)\top}$  and the foregoing task turns to calculate the  $k$ -largest eigenvectors  $Y$  of  $U^{(k)}U^{(k)\top}$ , which is exactly  $U^{(k)}$  as per the result in the follow lemma:

LEMMA 4.3. *The  $k$ -largest eigenvectors of  $U^{(k)}U^{(k)\top}$  is  $U^{(k)}$ .*

In a nutshell, our SCAG problem can be solved by (i) computing the top- $k$  left singular vectors  $Y$  of NSR  $Z$  and (ii) converting  $Y$  into a VCA  $C$  such that their distance is minimal. In the rest of this section, we elaborate on the algorithmic details of S<sup>2</sup>CAG that implement these steps.

### 4.2 Algorithm

The pseudo-code of S<sup>2</sup>CAG is illustrated in Algo. 1. S<sup>2</sup>CAG employs a fast rounding algorithm, SNEM [95, 98], to fulfil the second goal, i.e., derive  $\{C_1, C_2, \dots, C_k\}$  from  $Y$  (Line 14), whose runtime is merely  $O(kn)$ . The critical task thus lies on the computation of  $Y$ . A naive approach proceeds as follows. First, we construct the NSR using  $T$  power iterations [35], dubbed as PowerMethod<sup>2</sup>. It takes as input  $\hat{P}$ ,  $\hat{X}$ , order  $T$ , and decay factor  $\alpha$ , and outputs  $Z$  defined in Eq. (6) using  $O(dm)$  time per iteration. Next, we conduct the *randomized SVD* [32] of  $Z$  to get  $Y$ , which can be done in  $O(kdn)$  time. However, the cost  $O(Tdm)$  of constructing  $Z$  is significant on *dense* attributed graphs associated with large attribute sets. In such cases, a better treatment is to integrate the computation of  $Z$  into the process of the randomized SVD algorithm, so as to sidestep the explicit construction of  $Z$ .

S<sup>2</sup>CAG combines the aforementioned two ways in an adaptive fashion for optimal efficiency. More concretely, before entering the core procedure, S<sup>2</sup>CAG estimates the runtime costs of the naive and

<sup>2</sup>The pseudo-code appears in Appendix A.1.

**Algorithm 1:** S<sup>2</sup>CAG

---

**Input:** Attributed graph  $\mathcal{G}$ , the number  $k$  of clusters, order  $T$ , decay factor  $\alpha$ , the number  $\tau$  of iterations

**Output:** A set  $\{C_1, C_2, \dots, C_k\}$  of  $k$  clusters.

- 1 **if**  $f_{\text{naive}}(\mathcal{G}, k, \tau, T) \leq f_{\text{integr}}(\mathcal{G}, k, \tau, T)$  **then**
- 2      $Z \leftarrow \text{PowerMethod}(\hat{P}, \hat{X}, T, \alpha)$ ;
- 3     Compute  $Y'$  by the randomized SVD with  $k$  and  $o$ ;
- 4 **else**
- 5     Sample a Gaussian matrix  $R \sim \mathcal{N}(0, 1)^{d \times (k+o)}$ ;
- 6     **for**  $t \leftarrow 1$  **to**  $\tau$  **do**
- 7          $H \leftarrow \text{PowerMethod}(\hat{P}, \hat{X}R, T, \alpha)$ ;
- 8          $H \leftarrow \text{PowerMethod}(\hat{P}^\top, H, T, \alpha)$ ;
- 9          $R \leftarrow \hat{X}^\top H$ ;
- 10      $H \leftarrow \text{PowerMethod}(\hat{P}, \hat{X}R, T, \alpha)$ ;
- 11      $Q \leftarrow$  Orthogonal matrix by a QR factorization of  $H$ ;
- 12      $B \leftarrow \text{PowerMethod}(\hat{P}^\top, Q, T, \alpha)$ ;
- 13     Compute  $Y'$  according to Eq. (10);
- 14  $\{C_1, C_2, \dots, C_k\} \leftarrow$  Invoke SNEM with  $Y'_{\cdot, 2:k+1}$ ;

---

integrated approaches as the total amounts of matrix operations

$$\begin{aligned} f_{\text{integr}}(\mathcal{G}, k, \tau, T) &= 2(\tau + 1) \cdot (k + o) \cdot (dn + Tm) + 3(k + o)^2 n, \\ f_{\text{naive}}(\mathcal{G}, k, \tau, T) &= Tdm + 2(\tau + 1) \cdot (k + o)dn + 3(k + o)^2 n \end{aligned} \quad (9)$$

therein, respectively, based on  $\mathcal{G}$ , the number  $\tau$  of iterations, order  $T$ , and the number  $k$  of clusters. For the sake of space, we defer the complexity analysis to Appendix A.2.

If  $f_{\text{naive}}(\mathcal{G}, k, \tau, T) \leq f_{\text{integr}}(\mathcal{G}, k, \tau, T)$ , Algo. 1 follows the naive way remarked earlier (Lines 2-3), and otherwise integrates the computations of  $Z$  and  $Y$  (Lines 5-13). To be specific, it first generates a  $d \times (k + o)$  standard Gaussian random matrix  $R$  at Line 5, where  $o$  ( $o \geq 2$ ) stands for the oversampling parameter used in randomized SVD for proper conditioning. Next, we begin an iterative process to form  $H \leftarrow (ZZ^\top)^\tau ZR$  by calling `PowerMethod` with  $\hat{P}, \hat{X}R$  or  $\hat{P}^\top, H$  as inputs alternately at Lines 6-10.

Afterwards, S<sup>2</sup>CAG constructs an orthonormal matrix  $Q$  through a QR factorization of  $H$ , and feeds  $\hat{P}^\top$  and  $Q$  into `PowerMethod` to get a matrix  $B$  that builds  $Q^\top Z$  by  $B^\top \hat{X}$  (Lines 11-12). Lastly, we calculate  $Y'$  at Line 13 via

$$Y \leftarrow Q\Gamma, \text{ where } \Gamma \text{ is the left singular vectors of } B^\top \hat{X}. \quad (10)$$

**THEOREM 4.4.** *The columns of  $Y'$  computed at Line 13 in Algo. 1 are the approximate top- $(k + o)$  left singular vectors of  $Z$ .*

By Theorem 4.4,  $Y'$  derived in S<sup>2</sup>CAG contain the approximate top- $(k + o)$  left singular vectors of  $Z$ . Particularly, S<sup>2</sup>CAG selects the second to  $(k + 1)$ -th columns, i.e.,  $Y'_{\cdot, 2:k+1}$ , as  $Y$  for clustering. The reason is that  $ZZ^\top$  is close to a scaled stochastic matrix, rendering  $Y'_{\cdot, 1}$  approximate  $1/\sqrt{n}$  that is trivial for clustering. For the interest of space, we refer readers to Appendix A.3 for related evidence.

### 4.3 Theoretical Analysis

In S<sup>2</sup>CAG, the VCA matrix  $C$  is obtained via SNEM [95] with  $Y$ , whose goal is to find a VCA matrix  $C$  such that

$$\min_{T \in \mathbb{R}^{k \times k}} \|YT - C\|_2 \text{ subject to } TT^\top = I$$

is optimized, i.e., the distance between  $YT$  and  $C$  is minimized. Ideally, the optimum  $C^*$  satisfies  $C^* = YT$  and  $TT^\top = I$ , which leads to

$$\begin{aligned} \text{trace}(C^{*\top} ZZ^\top C^*) &= \text{trace}(T^\top Y^\top ZZ^\top YT) \\ &= \text{trace}(Y^\top ZZ^\top YTT^\top) = \text{trace}(Y^\top ZZ^\top Y). \end{aligned}$$

**LEMMA 4.5.**  $Y = \arg \max_{Y \in \mathbb{R}^{n \times k}} \text{trace}(Y^\top ZZ^\top Y)$  subject to  $Y^\top Y = I$ .

Since  $Y$  is an optimal solution to the trace maximization problem in Lemma 4.5, the optimal VCA  $C^*$  that S<sup>2</sup>CAG aims to derive also maximizes  $\text{trace}(C^\top ZZ^\top C)$  where  $C$  is required to be a VCA defined in Eq. (8). Put another way, the objective of S<sup>2</sup>CAG is equivalent to optimizing the problem of  $\max_C \text{trace}(C^\top ZZ^\top C)$ .

**LEMMA 4.6.** *Let  $\tilde{\mathcal{G}}$  be an undirected weighted graph with vertex set  $\mathcal{V}$  and adjacency matrix  $W$ , wherein each entry  $W_{i,j}$  stands for the weight of edge  $(v_i, v_j) \in \tilde{\mathcal{G}}$ . If there exists a scalar  $\beta$  such that  $\beta \cdot W$  is a stochastic matrix,*

$$\max_C \text{trace}(C^\top W^\top C) \Leftrightarrow \min_{\{C_1, C_2, \dots, C_k\}} \phi(C_1, C_2, \dots, C_k)$$

holds and  $\phi(C_1, C_2, \dots, C_k)$  denotes the total conductance [57] of clusters  $\{C_1, C_2, \dots, C_k\}$ , i.e.,

$$\phi(C_1, C_2, \dots, C_k) = \sum_{\ell=1}^k \sum_{v_i \in C_\ell, v_j \in \mathcal{V} \setminus C_\ell} \frac{W_{i,j}}{|C_\ell|}. \quad (11)$$

Let  $\tilde{\mathcal{G}}$  be an affinity graph constructed on the vertex set  $\mathcal{V}$  and every edge  $(v_i, v_j) \in \mathcal{V} \times \mathcal{V}$  is associated with a weight computed by  $Z_i \cdot Z_j$ . Accordingly,  $ZZ^\top$  is the weighted adjacency matrix of  $\tilde{\mathcal{G}}$ , which is approximately stochastic as pinpointed in the preceding section. Lemma 4.6 implies that S<sup>2</sup>CAG is to partition vertices in  $\tilde{\mathcal{G}}$  into  $k$  clusters  $\{C_1, C_2, \dots, C_k\}$  such that their total conductance (i.e., the overall connectivity of vertices across clusters over  $\tilde{\mathcal{G}}$ ) defined in Eq. (11) is minimized.

## 5 MODULARITY-BASED S<sup>2</sup>CAG APPROACH

Aside from conductance, *modularity* introduced by Newman [69] is another prominent and eminently useful metric for vertex clustering over graphs. Inspired by our theoretical finding in Section 4.3, this section investigates incorporating the *modularity* maximization objective into the S<sup>2</sup>CAG framework and devises M-S<sup>2</sup>CAG for SCAG computation.

### 5.1 High-level Idea

In a fully random graph model, the probability that vertex  $v_i$  is connected to  $v_j$  is  $\frac{d(v_i) \cdot d(v_j)}{2m}$ . Given  $\mathcal{G}$  and a clustering  $\{C_1, C_2, \dots, C_k\}$ , the modularity [69] of  $\{C_1, C_2, \dots, C_k\}$  on  $\mathcal{G}$  measures the deviation of the intra-cluster connectivity on  $\mathcal{G}$  from what would be observed in expectation when edges in  $\mathcal{G}$  are randomly populated:

$$Q = \frac{1}{2m} \sum_{\ell=1}^k \sum_{v_i, v_j \in C_\ell} A_{i,j} - \frac{d(v_i) \cdot d(v_j)}{2m}.$$

Modularity-based clustering aims to find a division  $\{C_1, C_2, \dots, C_k\}$  of  $\mathcal{G}$  that maximizes modularity  $Q$ .

**Algorithm 2: M-S<sup>2</sup>CAG**


---

**Input:**  $\mathcal{G}, k, T, \alpha, \gamma, \tau$   
**Output:** A set of  $k$  clusters  $\{C_1, C_2, \dots, C_k\}$

- 1  $Z \leftarrow \text{PowerMethod}(\hat{P}, \hat{X}, T, \alpha)$ ;
- 2 Compute  $\hat{Z}$  and  $\omega$  by Eq. (13);
- 3 Sample a Gaussian matrix  $R \sim \mathcal{N}(0, 1)^{n \times k}$ ;
- 4  $Q \leftarrow$  Orthogonal matrix by a QR factorization of  $R$ ;
- 5 **for**  $i \leftarrow 1$  **to**  $\tau$  **do**
- 6     Compute  $H$  according to Eq. (15);
- 7      $Q \leftarrow$  Orthogonal matrix by a QR factorization of  $H$ ;
- 8  $\{C_1, C_2, \dots, C_k\} \leftarrow$  Invoke SNEM with  $Q$ ;

---

Akin to the conductance minimization objective in S<sup>2</sup>CAG (Section 4.3), we extend the modularity definition to the weighted graph  $\hat{\mathcal{G}}$  constructed based on NSR  $Z$  and formulate  $Q$  over  $\hat{\mathcal{G}}$  as follows:

$$Q = \frac{1}{\omega^\top \mathbf{1}} \sum_{\ell=1}^k \sum_{v_i, v_j \in C_\ell} W_{i,j} - \gamma \cdot \frac{\omega_i \cdot \omega_j}{\omega^\top \mathbf{1}}, \quad (12)$$

where  $\gamma$  is a weight parameter for the second term.  $W_{i,j}$  denotes the weight of each edge  $(v_i, v_j) \in \mathcal{V} \times \mathcal{V}$

$$W_{i,j} = \hat{Z}_i \cdot \hat{Z}_j^\top \text{ where } \hat{Z}_i = \frac{Z_i}{\sqrt{\sum_{v_j \in \mathcal{V}} Z_i \cdot Z_j^\top}} \quad \forall v_i \in \mathcal{V}, \quad (13)$$

and  $\omega \in \mathbb{R}^n$  is a length- $n$  column vector where each entry  $\omega_i = \sum_{v_j \in \mathcal{V}} W_{i,j} \quad \forall v_i \in \mathcal{V}$ . Unlike S<sup>2</sup>CAG, we leverage the normalized version  $\hat{Z}$  of  $Z$  for edge weighting in affinity graph  $\hat{\mathcal{G}}$  as  $\hat{Z}\hat{Z}^\top$  is approximately stochastic as pinpointed previously, which makes  $\omega$  an all-one vector and thus the term  $\gamma \frac{\omega_i \cdot \omega_j}{\omega^\top \mathbf{1}}$  in  $Q$  ineffectual.

**LEMMA 5.1.** *Given  $k$  clusters  $\{C_1, C_2, \dots, C_k\}$ , whose corresponding vertex-cluster indicator is  $C \in \mathbb{R}^{n \times k}$  where  $C_{i,j} = 1$  if  $v_i \in C_j$  and 0 otherwise. If the following trace maximization problem is optimized*

$$\max_C \text{trace} \left( C^\top \left( \hat{Z}\hat{Z}^\top - \gamma \cdot \frac{\omega\omega^\top}{\omega^\top \mathbf{1}} \right) C \right), \quad (14)$$

$\{C_1, C_2, \dots, C_k\}$  maximizes the modularity  $Q$  defined on  $\hat{\mathcal{G}}$  in Eq. (12).

Lemma 5.1 establishes an equivalence between our modularity-based objective in Eq. (12) and the trace maximization problem in Eq. (14). By relaxing  $C$  and leveraging Ky Fan's trace maximization principle [25], the matrix  $C$  optimizing Eq. (14) is the  $k$ -largest eigenvectors  $Y$  of  $\hat{Z}\hat{Z}^\top - \gamma \cdot \frac{\omega\omega^\top}{\omega^\top \mathbf{1}}$ . Analogous to S<sup>2</sup>CAG, the clusters  $\{C_1, C_2, \dots, C_k\}$  thus can be extracted from  $Y$  through SNEM.

Instead of materializing the  $n \times n$  dense matrix  $\hat{Z}\hat{Z}^\top - \gamma \cdot \frac{\omega\omega^\top}{\omega^\top \mathbf{1}}$  for the computation of  $Y$ , the idea of M-S<sup>2</sup>CAG is to harness the fact that the matrix-vector product  $(\hat{Z}\hat{Z}^\top - \gamma \cdot \frac{\omega\omega^\top}{\omega^\top \mathbf{1}}) \cdot \mathbf{q}$  in iterative eigenvalue solvers can be reordered as  $\hat{Z} \cdot (\hat{Z}^\top \mathbf{q} - \gamma \cdot \frac{\omega}{\omega^\top \mathbf{1}} \cdot (\omega^\top \mathbf{q}))$  and done in  $O(dn)$  time.

## 5.2 Algorithm and Analysis

Algo. 2 presents the pseudo-code of M-S<sup>2</sup>CAG, which begins by taking an additional parameter  $\gamma$  compared to Algo. 1. Initially, M-S<sup>2</sup>CAG obtains NSR  $Z$  via PowerMethod, based on which it calculates  $\hat{Z}$  and  $\omega$  as in the context of Eq. (13) (Lines 1-2). At Lines 3-4, we create an  $n \times k$  orthogonal matrix  $Q$  through a QR decomposition of a standard Gaussian matrix  $R \in \mathbb{R}^{n \times k}$  generated randomly. Subsequently, M-S<sup>2</sup>CAG performs  $\tau$  subspace iterations [76] to update

**Table 1: Statistics of Datasets.**

Dataset	#Vertices	#Edges	#Attributes	#Clusters
<i>CiteSeer</i>	3,327	4,732	3,703	6
<i>Wiki</i>	2,405	14,001	4,973	17
<i>ACM</i>	3,025	16,153	1,870	3
<i>Photo</i>	7,487	119,043	745	8
<i>Cora</i>	19,793	63,421	8,710	70
<i>PubMed</i>	19,717	64,041	500	3
<i>DBLP</i>	4,057	2,502,276	334	4
<i>ArXiv</i>	169,343	1,327,142	128	40

$Q$ , each of which first calculates  $H$  at Line 6 by

$$H \leftarrow \hat{Z} \cdot (\hat{Z}^\top Q) - \gamma \cdot \frac{\omega}{\omega^\top \mathbf{1}} \cdot (\omega^\top Q), \quad (15)$$

and then at Line 7 updates  $Q$  as the orthogonal matrix from the QR factorization of  $H$ . The final  $Q$  will be used as  $Y$  input to SNEM for outputting clusters  $\{C_1, C_2, \dots, C_k\}$ .

**THEOREM 5.2.** *When  $Q$  in Algo. 2 converges, the columns of  $Q$  are the  $k$ -largest eigenvectors of  $\hat{Z}\hat{Z}^\top - \gamma \cdot \frac{\omega\omega^\top}{\omega^\top \mathbf{1}}$  and  $S = QQ^\top$  optimizes*

$$\min_{\text{rank}(S)=k} \|\tilde{Z} - S\tilde{Z}\|_F^2 + \|S^\top S - I\|_F^2, \quad (16)$$

where  $\tilde{Z}$  satisfies  $\tilde{Z}\tilde{Z}^\top = \hat{Z}\hat{Z}^\top - \gamma \cdot \frac{\omega\omega^\top}{\omega^\top \mathbf{1}}$ .

Theorem 5.2 proves the correctness of M-S<sup>2</sup>CAG and manifests that the objective function of M-S<sup>2</sup>CAG from the perspective of subspace clustering can be formulated as Eq. (16) based on NSR  $\tilde{Z}$  ensuring  $\tilde{Z}\tilde{Z}^\top = \hat{Z}\hat{Z}^\top - \gamma \cdot \frac{\omega\omega^\top}{\omega^\top \mathbf{1}}$ .

## 6 EXPERIMENTS

This section experimentally evaluates S<sup>2</sup>CAG and M-S<sup>2</sup>CAG against 17 competitors regarding clustering quality and efficiency on 8 real attributed graphs. All experiments are conducted on a Linux machine with an NVIDIA Ampere A100 GPU (80GB memory), AMD EPYC 7513 CPUs (2.6 GHz), and 1TB RAM. Due to space constraint, we defer the clustering visualizations to Appendix B.

### 6.1 Experimental Setup

**Datasets.** Table 1 summarizes the statistics of datasets we experiment with. *CiteSeer*, *PubMed* [78], *Cora* [6], *ACM*, *DBLP* [92], and *ArXiv* [36] are academic citation networks, in which ground-truth clusters represent subjects or fields of study of publications. *Photo* is a segment of the Amazon product co-purchase graph [65], where cluster labels correspond to product categories. *Wiki* [94] is a reference network of Wikipedia documents.

**Evaluation Criteria.** Following previous works [3, 9, 28, 54, 84], we adopt three widely-used metrics: *Clustering Accuracy* (ACC), *Normalized Mutual Information* (NMI), and *Adjusted Rand Index* (ARI) to assess the clustering quality in the presence of ground-truth cluster labels. ACC and NMI scores range from 0 to 1.0, whilst ARI ranges from -0.5 to 1.0. For all of them, higher values indicate better clustering performance.

**Baselines, Implementations, and Parameter Settings.** We carefully select 17 competing methods from four categories for comparison including one metric clustering method KMeans [42]; five subspace clustering methods: K-FSC [24], LSR [58], SSC-OMP [13], EDESC [9], SAGSC [28]; four spectral methods: SC [80], MinCut-Pool [4], DMoN [84], DGCluster [3]; and seven GRL-based methods:

Table 2: Clustering Quality on ACM, Wiki, CiteSeer, and Photo.

Method	ACM			Wiki			CiteSeer			Photo			Rank
	ACC $\uparrow$	NMI $\uparrow$	ARI $\uparrow$	ACC $\uparrow$	NMI $\uparrow$	ARI $\uparrow$	ACC $\uparrow$	NMI $\uparrow$	ARI $\uparrow$	ACC $\uparrow$	NMI $\uparrow$	ARI $\uparrow$	
KMeans [42]	88.7 $\pm$ 0.9	63.3 $\pm$ 1.7	69.4 $\pm$ 2.2	45.6 $\pm$ 2.9	46.9 $\pm$ 2.1	26.1 $\pm$ 2.5	29.84 $\pm$ 1.8	39.8 $\pm$ 0.5	36.8 $\pm$ 0.7	43.8 $\pm$ 1.6	34.3 $\pm$ 0.8	23.6 $\pm$ 1.0	11.2
K-FSC [24]	70.5 $\pm$ 0.0	28.1 $\pm$ 0.0	31.3 $\pm$ 0.0	47.2 $\pm$ 1.2	44.1 $\pm$ 1.9	27.8 $\pm$ 1.8	18.5 $\pm$ 0.0	0.0 $\pm$ 0.0	0.0 $\pm$ 0.0	47.7 $\pm$ 0.0	23.3 $\pm$ 0.0	18.5 $\pm$ 0.0	13.6
LSR [58]	60.3 $\pm$ 0.0	2.1 $\pm$ 0.0	3.7 $\pm$ 0.0	7.4 $\pm$ 0.0	2.5 $\pm$ 0.0	0.1 $\pm$ 0.0	18.5 $\pm$ 3.1	0.0 $\pm$ 0.0	0.0 $\pm$ 0.0	3.2 $\pm$ 0.0	33.5 $\pm$ 0.0	12.7 $\pm$ 0.0	17.5
SSC-OMP [13]	81.5 $\pm$ 0.0	47.6 $\pm$ 0.0	53.6 $\pm$ 0.0	42.6 $\pm$ 2.1	38.4 $\pm$ 0.9	24.4 $\pm$ 1.2	22.7 $\pm$ 3.1	2.7 $\pm$ 3.1	1.3 $\pm$ 2.1	60.0 $\pm$ 0.1	49.9 $\pm$ 0.4	40.9 $\pm$ 0.3	14.5
EDESC [9]	82.5 $\pm$ 0.0	52.9 $\pm$ 0.0	56.1 $\pm$ 0.0	40.9 $\pm$ 0.0	37.5 $\pm$ 0.0	20.2 $\pm$ 0.0	42.9 $\pm$ 0.0	19.8 $\pm$ 0.0	16.0 $\pm$ 0.0	38.8 $\pm$ 0.0	26.8 $\pm$ 0.0	16.8 $\pm$ 0.0	15.3
SAGSC [28]	93.2 $\pm$ 0.0	75.1 $\pm$ 0.1	80.9 $\pm$ 0.1	55.1 $\pm$ 2.2	52.5 $\pm$ 1.0	32.5 $\pm$ 2.6	67.7 $\pm$ 0.0	42.9 $\pm$ 0.1	43.5 $\pm$ 0.1	77.9 $\pm$ 0.0	71.9 $\pm$ 0.0	60.2 $\pm$ 0.0	3.8
SC [80]	84.5 $\pm$ 0.0	53.7 $\pm$ 0.1	59.7 $\pm$ 0.0	19.9 $\pm$ 2.1	8.5 $\pm$ 2.4	0.2 $\pm$ 0.2	20.9 $\pm$ 0.0	1.4 $\pm$ 0.0	0.0 $\pm$ 0.0	75.1 $\pm$ 0.0	59.7 $\pm$ 0.0	54.4 $\pm$ 0.0	15.0
MinCutPool [4]	89.8 $\pm$ 0.0	65.6 $\pm$ 0.0	71.8 $\pm$ 0.0	44.0 $\pm$ 0.0	38.8 $\pm$ 0.0	24.1 $\pm$ 0.0	40.4 $\pm$ 0.0	21.5 $\pm$ 0.0	16.7 $\pm$ 0.0	25.4 $\pm$ 0.0	0.2 $\pm$ 0.0	0.0 $\pm$ 0.0	11.6
DMoN [84]	34.5 $\pm$ 0.1	0.4 $\pm$ 0.0	0.1 $\pm$ 0.0	52.2 $\pm$ 0.0	47.4 $\pm$ 0.0	32.2 $\pm$ 0.1	30.6 $\pm$ 0.1	26.5 $\pm$ 0.0	16.8 $\pm$ 0.0	23.9 $\pm$ 0.3	9.8 $\pm$ 0.3	4.1 $\pm$ 0.2	13.0
DGCluster [3]	68.2 $\pm$ 0.0	62.9 $\pm$ 0.0	58.2 $\pm$ 0.0	56.4 $\pm$ 0.0	50.2 $\pm$ 0.0	40.6 $\pm$ 0.0	39.8 $\pm$ 0.0	41.1 $\pm$ 0.0	27.1 $\pm$ 0.0	72.0 $\pm$ 0.0	70.7 $\pm$ 0.0	58.0 $\pm$ 0.0	7.2
GCC [27]	65.3 $\pm$ 0.0	55.0 $\pm$ 0.1	48.0 $\pm$ 0.0	54.8 $\pm$ 0.0	55.1 $\pm$ 0.0	33.8 $\pm$ 0.0	69.4 $\pm$ 0.0	45.1 $\pm$ 0.0	45.5 $\pm$ 0.0	59.7 $\pm$ 2.2	61.1 $\pm$ 5.0	38.7 $\pm$ 1.7	6.2
GIC [64]	90.7 $\pm$ 0.0	70.7 $\pm$ 0.0	73.5 $\pm$ 0.0	44.2 $\pm$ 0.0	44.7 $\pm$ 0.0	28.3 $\pm$ 0.0	68.3 $\pm$ 0.0	44.5 $\pm$ 0.0	46.0 $\pm$ 0.0	65.6 $\pm$ 0.1	59.7 $\pm$ 0.0	47.9 $\pm$ 0.0	8.3
SSGC [108]	86.9 $\pm$ 0.0	61.2 $\pm$ 0.0	65.7 $\pm$ 0.0	50.5 $\pm$ 0.0	47.7 $\pm$ 0.0	27.4 $\pm$ 0.0	69.0 $\pm$ 0.0	42.8 $\pm$ 0.0	44.4 $\pm$ 0.0	57.7 $\pm$ 0.1	61.2 $\pm$ 0.0	33.8 $\pm$ 0.0	7.8
SDCN [5]	89.8 $\pm$ 0.0	66.4 $\pm$ 0.0	72.2 $\pm$ 0.0	36.5 $\pm$ 0.0	31.7 $\pm$ 0.0	16.5 $\pm$ 0.0	47.0 $\pm$ 0.1	23.4 $\pm$ 0.0	18.7 $\pm$ 0.1	53.4 $\pm$ 0.1	40.8 $\pm$ 0.1	31.8 $\pm$ 0.1	11.9
DCRN [55]	89.3 $\pm$ 0.0	65.5 $\pm$ 0.0	70.8 $\pm$ 0.0	51.6 $\pm$ 0.0	49.4 $\pm$ 0.0	22.4 $\pm$ 0.0	70.6 $\pm$ 0.0	45.6 $\pm$ 0.0	47.6 $\pm$ 0.1	75.7 $\pm$ 0.1	70.7 $\pm$ 0.1	57.3 $\pm$ 0.1	6.5
DAEGC [88]	90.1 $\pm$ 0.0	67.6 $\pm$ 0.0	73.1 $\pm$ 0.0	45.7 $\pm$ 0.0	41.9 $\pm$ 0.0	25.8 $\pm$ 0.0	68.4 $\pm$ 0.0	43.9 $\pm$ 0.0	44.4 $\pm$ 0.0	41.4 $\pm$ 0.0	36.5 $\pm$ 0.0	13.4 $\pm$ 0.0	9.1
Dink-Net [54]	62.2 $\pm$ 0.0	27.1 $\pm$ 0.0	23.2 $\pm$ 0.0	42.9 $\pm$ 0.0	35.7 $\pm$ 0.0	21.3 $\pm$ 0.0	67.6 $\pm$ 0.0	32.4 $\pm$ 0.0	32.1 $\pm$ 0.0	71.4 $\pm$ 0.0	59.7 $\pm$ 0.0	49.7 $\pm$ 0.0	11.7
S <sup>2</sup> CAG (SNEM)	93.5 $\pm$ 0.0	75.4 $\pm$ 0.0	81.4 $\pm$ 0.0	64.4 $\pm$ 0.0	55.1 $\pm$ 0.0	44.9 $\pm$ 0.0	72.2 $\pm$ 0.0	45.6 $\pm$ 0.0	48.5 $\pm$ 0.0	78.9 $\pm$ 0.0	69.0 $\pm$ 0.0	58.9 $\pm$ 0.1	2.0
M-S <sup>2</sup> CAG (SNEM)	93.7 $\pm$ 0.0	76.0 $\pm$ 0.0	82.0 $\pm$ 0.0	60.2 $\pm$ 0.0	51.1 $\pm$ 0.0	37.8 $\pm$ 0.0	72.2 $\pm$ 0.0	45.2 $\pm$ 0.0	48.2 $\pm$ 0.0	79.2 $\pm$ 0.0	71.1 $\pm$ 0.0	59.7 $\pm$ 0.0	1.7

Table 3: Clustering Quality on DBLP, PubMed, Cora, and ArXiv.

Method	DBLP			PubMed			Cora			ArXiv			Rank
	ACC $\uparrow$	NMI $\uparrow$	ARI $\uparrow$	ACC $\uparrow$	NMI $\uparrow$	ARI $\uparrow$	ACC $\uparrow$	NMI $\uparrow$	ARI $\uparrow$	ACC $\uparrow$	NMI $\uparrow$	ARI $\uparrow$	
KMeans [42]	68.1 $\pm$ 0.2	37.3 $\pm$ 0.2	31.87 $\pm$ 0.5	59.2 $\pm$ 0.1	30.0 $\pm$ 0.1	26.6 $\pm$ 0.1	29.8 $\pm$ 1.8	39.8 $\pm$ 0.5	10.5 $\pm$ 0.4	17.0 $\pm$ 0.2	22.6 $\pm$ 0.1	7.3 $\pm$ 0.1	11.2
K-FSC [24]	42.0 $\pm$ 0.0	13.2 $\pm$ 0.0	10.3 $\pm$ 0.0	55.4 $\pm$ 0.1	16.5 $\pm$ 0.0	15.7 $\pm$ 0.0	23.9 $\pm$ 0.0	29.8 $\pm$ 0.0	11.0 $\pm$ 0.0	17.3 $\pm$ 0.0	15.5 $\pm$ 0.0	6.1 $\pm$ 0.0	13.6
LSR [58]	30.9 $\pm$ 0.2	1.1 $\pm$ 0.1	0.3 $\pm$ 0.1	38.8 $\pm$ 0.0	0.4 $\pm$ 0.0	0.6 $\pm$ 0.0	1.8 $\pm$ 0.0	0.1 $\pm$ 0.0	0.0 $\pm$ 0.0	6.3 $\pm$ 0.0	0.5 $\pm$ 0.0	0.0 $\pm$ 0.0	17.5
SSC-OMP [13]	29.5 $\pm$ 0.1	0.2 $\pm$ 0.1	-0.1 $\pm$ 0.0	60.3 $\pm$ 0.0	21.5 $\pm$ 0.0	18.9 $\pm$ 0.0	13.8 $\pm$ 0.2	22.6 $\pm$ 0.1	6.3 $\pm$ 0.1	-	-	-	14.5
EDESC [9]	44.5 $\pm$ 0.1	12.8 $\pm$ 0.1	12.3 $\pm$ 0.1	47.8 $\pm$ 0.0	3.8 $\pm$ 0.0	3.1 $\pm$ 0.0	10.5 $\pm$ 0.0	15.2 $\pm$ 0.0	2.9 $\pm$ 0.0	-	-	-	15.3
SAGSC [28]	93.1 $\pm$ 0.1	78.0 $\pm$ 0.2	83.3 $\pm$ 0.3	71.1 $\pm$ 0.0	32.9 $\pm$ 0.0	34.1 $\pm$ 0.0	41.3 $\pm$ 0.9	53.9 $\pm$ 0.9	24.4 $\pm$ 1.3	47.8 $\pm$ 1.8	46.9 $\pm$ 0.6	38.2 $\pm$ 0.7	3.8
SC [80]	30.0 $\pm$ 0.0	1.4 $\pm$ 0.0	0.1 $\pm$ 0.0	53.8 $\pm$ 0.0	10.8 $\pm$ 0.0	7.2 $\pm$ 0.0	10.2 $\pm$ 0.5	16.3 $\pm$ 1.0	2.0 $\pm$ 0.2	-	-	-	15.0
MiniCutPool [4]	87.7 $\pm$ 0.1	71.8 $\pm$ 0.0	74.1 $\pm$ 0.0	61.5 $\pm$ 0.0	28.3 $\pm$ 0.0	25.4 $\pm$ 0.0	31.0 $\pm$ 0.0	49.5 $\pm$ 0.0	19.1 $\pm$ 0.0	-	-	-	11.6
DMoN [84]	46.3 $\pm$ 0.6	57.3 $\pm$ 0.1	38.4 $\pm$ 0.5	21.7 $\pm$ 0.0	22.6 $\pm$ 0.0	9.5 $\pm$ 0.0	23.3 $\pm$ 0.0	42.7 $\pm$ 0.0	16.4 $\pm$ 0.0	37.5 $\pm$ 0.0	38.6 $\pm$ 0.0	27.4 $\pm$ 0.0	13.0
DGCluster [3]	92.1 $\pm$ 0.1	75.2 $\pm$ 0.0	80.9 $\pm$ 0.0	41.4 $\pm$ 0.0	34.7 $\pm$ 0.0	24.4 $\pm$ 0.0	38.1 $\pm$ 0.0	53.4 $\pm$ 0.0	28.0 $\pm$ 0.0	33.9 $\pm$ 0.0	43.2 $\pm$ 0.0	29.2 $\pm$ 0.0	7.2
GCC [27]	90.9 $\pm$ 1.1	73.6 $\pm$ 0.0	78.4 $\pm$ 2.2	70.8 $\pm$ 2.2	32.3 $\pm$ 4.1	33.3 $\pm$ 0.0	40.2 $\pm$ 0.0	54.1 $\pm$ 0.0	26.0 $\pm$ 0.0	41.2 $\pm$ 0.0	47.1 $\pm$ 0.0	35.8 $\pm$ 0.0	6.2
GIC [64]	87.4 $\pm$ 0.0	68.1 $\pm$ 0.0	71.7 $\pm$ 0.0	65.1 $\pm$ 0.0	26.4 $\pm$ 0.0	24.6 $\pm$ 0.0	30.6 $\pm$ 0.0	50.2 $\pm$ 0.0	20.0 $\pm$ 0.0	12.4 $\pm$ 0.0	18.4 $\pm$ 0.0	6.4 $\pm$ 0.0	8.3
SSGC [108]	87.1 $\pm$ 0.0	67.5 $\pm$ 0.0	71.6 $\pm$ 0.0	70.7 $\pm$ 0.0	32.5 $\pm$ 4.5	33.3 $\pm$ 0.0	37.0 $\pm$ 0.0	53.6 $\pm$ 0.0	26.0 $\pm$ 0.0	28.9 $\pm$ 0.0	32.0 $\pm$ 0.0	20.0 $\pm$ 0.0	7.8
SDCN [5]	79.4 $\pm$ 0.1	58.3 $\pm$ 0.0	58.7 $\pm$ 0.1	63.0 $\pm$ 0.0	23.4 $\pm$ 0.0	22.2 $\pm$ 0.0	11.5 $\pm$ 0.0	21.1 $\pm$ 0.0	4.2 $\pm$ 0.0	26.4 $\pm$ 0.0	17.8 $\pm$ 0.0	10.5 $\pm$ 0.0	11.9
DCRN [55]	93.0 $\pm$ 0.0	77.8 $\pm$ 0.0	83.5 $\pm$ 0.0	69.0 $\pm$ 0.0	34.2 $\pm$ 0.0	32.1 $\pm$ 0.0	39.4 $\pm$ 0.0	53.3 $\pm$ 0.0	26.5 $\pm$ 0.0	-	-	-	6.5
DAEGC [88]	89.8 $\pm$ 0.0	71.2 $\pm$ 0.0	76.1 $\pm$ 0.0	65.2 $\pm$ 0.0	25.8 $\pm$ 0.0	24.6 $\pm$ 0.0	32.2 $\pm$ 0.0	49.9 $\pm$ 0.0	21.3 $\pm$ 0.0	-	-	-	9.1
Dink-Net [54]	87.3 $\pm$ 0.1	67.1 $\pm$ 0.0	69.7 $\pm$ 0.0	66.1 $\pm$ 0.0	25.7 $\pm$ 0.0	25.9 $\pm$ 0.0	32.9 $\pm$ 0.0	39.3 $\pm$ 0.0	15.8 $\pm$ 0.0	20.5 $\pm$ 0.0	17.6 $\pm$ 0.0	7.1 $\pm$ 0.0	11.7
S <sup>2</sup> CAG (SNEM)	93.5 $\pm$ 0.0	78.8 $\pm$ 0.0	84.3 $\pm$ 0.0	75.3 $\pm$ 0.0	36.5 $\pm$ 0.0	41.9 $\pm$ 0.0	44.7 $\pm$ 0.0	53.6 $\pm$ 0.0	33.1 $\pm$ 0.0	46.9 $\pm$ 0.0	46.1 $\pm$ 0.0	38.7 $\pm$ 0.0	2.0
M-S <sup>2</sup> CAG (SNEM)	93.5 $\pm$ 0.0	78.9 $\pm$ 0.0	84.3 $\pm$ 0.0	75.5 $\pm$ 0.0	36.8 $\pm$ 0.0	42.3 $\pm$ 0.0	44.4 $\pm$ 0.0	53.9 $\pm$ 0.0	31.6 $\pm$ 0.0	50.0 $\pm$ 0.0	47.2 $\pm$ 0.0	40.5 $\pm$ 0.0	1.7

GCC [27], GIC [64], SSGC [108], SDCN [5], DCRN [55], DAEGC [88], Dink-Net [54]. Amid them, metric clustering and subspace clustering methods are solely applied to attribute matrices, except SAGSC, which is a SCAG solution using hand-crafted features from graph structures and attributes. Spectral methods produce clusters by optimizing conductance- or modularity-like metrics on the original graph, while GRL-based approaches apply KMeans to vertex representations learned by various neural network models.

For most competitors, we reproduce results using source codes collected from authors and parameter settings prescribed when possible. Unless otherwise specified, we set  $\gamma$  in M-S<sup>2</sup>CAG to 0.9 on CiteSeer and Wiki and 1.0 on others. As for the numbers  $\tau$  of iterations in S<sup>2</sup>CAG and M-S<sup>2</sup>CAG, we follow the default settings in randomized SVD and subspace iterations. We run grid searches for remaining parameters (i.e.,  $\alpha$  and  $T$ ) and report the best results. More details regarding parameter setup are in Appendix B. The datasets and our code are available at <https://github.com/HKBU-LAGAS/S2CAG>.

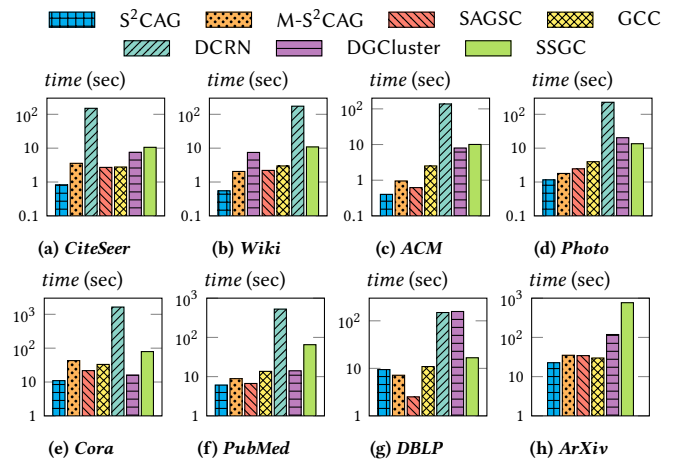


Figure 1: Clustering efficiency performance.

## 6.2 Performance Evaluation

**6.2.1 Clustering Quality.** This set of experiments reports the ACC, NMI, and ARI scores achieved by  $S^2CAG$ ,  $M-S^2CAG$ , and all baselines over 8 datasets. We conduct 5 trials and report the averaged values and standard deviation over the trials. A method is omitted if it fails to report the results within one day or incurs out-of-memory errors.

Tables 2 and 3 show the ACC, NMI, ARI scores, and the average performance rankings. The best and second-best results are highlighted in blue and darker shades indicate better clustering. The best baselines are underlined. From the last columns of Tables 2 and 3, we can see that  $M-S^2CAG$  and  $S^2CAG$  are ranked the highest and second highest in terms of overall clustering quality among all evaluated methods, respectively, whereas the best performer SAGSC [28] in baselines is another SCAG approach. This observation validates the effectiveness of subspace clustering for attributed graph clustering tasks.

Specifically, on small and medium-sized attributed graphs,  $S^2CAG$  and  $M-S^2CAG$  outperform all competing methods, with conspicuous improvements pertinent to almost all metrics. For instance, our proposed methods improve the best baselines by significant margins of 8%, 4.9%, 4.3% in ACC, NMI, and ARI on *Wiki*, and 4.4%, 2.1%, 8.2% on *PubMed*, respectively. This superiority is still pronounced on datasets with millions of edges, i.e., *DBLP* and *ArXiv*, where we can observe that  $M-S^2CAG$  is able to give a performance gain of 0.4%, 2.2% for ACC and 1.0%, 2.3% for ARI, respectively. Moreover, on all datasets except a small one *Wiki*, it can be observed that  $M-S^2CAG$  yields comparable and often superior performance to  $S^2CAG$ . Overall,  $M-S^2CAG$  improves  $S^2CAG$  in generalization and robustness by maximizing modularity.

**6.2.2 Efficiency.** Fig. 1 depicts the running times required by  $S^2CAG$ ,  $M-S^2CAG$ , and other competitive baselines (ranked top 7 in Tables 2 and 3) for clustering on all datasets. The  $y$ -axis represents the running time (seconds) in log scale. The reported runtime values exclude the costs for input (loading datasets) and output (saving clustering results).

From Fig. 1(a) and 1(b), we can observe that  $S^2CAG$  is able to gain 183 $\times$  and 13.6 $\times$  speedup on *CiteSeer* and *Wiki* when compared to the best baselines DCRN and DGCluster, respectively. On the rest of the datasets except *DBLP*,  $S^2CAG$  and  $M-S^2CAG$  achieve comparable efficiency to the state of the art SAGSC and are among the fastest methods. Over the *DBLP* graph with 2.5 million edges, our solutions take at least 7.2 seconds to terminate and SAGSC consumes 2.5 seconds. But recall that in Table 3,  $S^2CAG$  and  $M-S^2CAG$  outperform SAGSC by a considerable gain of 0.4%, 0.8%, 1.0% in ACC, NMI, and ARI, respectively.

In summary,  $S^2CAG$  and  $M-S^2CAG$  consistently deliver superior results for clustering on various attributed graphs while offering high empirical efficiency. The empirical observation corroborates the efficacy of our novel objective function in Section 3.4 and algorithmic designs developed in Sections 4 and Section 5.

## 6.3 Parameter Study

This set of experiments investigates the effects of parameters  $\alpha$ ,  $T$ , and  $\gamma$  in  $S^2CAG$  and  $M-S^2CAG$ . We run  $S^2CAG$  and  $M-S^2CAG$  on

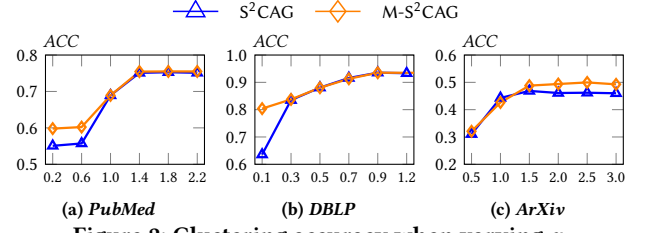


Figure 2: Clustering accuracy when varying  $\alpha$

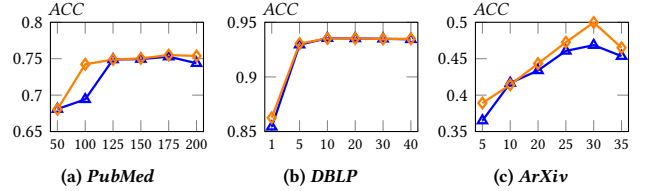


Figure 3: Clustering accuracy when varying  $T$ .

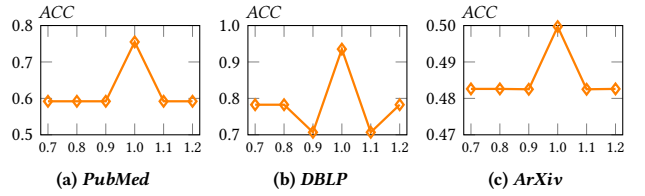


Figure 4: Varying  $\gamma$  in  $M-S^2CAG$

the three largest datasets *PubMed*, *DBLP*, and *ArXiv*, respectively, by varying each parameter while fixing others as in Section 6.1.

**Varying  $\alpha$ .** Fig. 2 illustrates the ACC scores obtained by  $S^2CAG$  and  $M-S^2CAG$  on *PubMed*, *DBLP*, and *ArXiv* when  $\alpha$  is varied from 0.2 to 2.2, 0.1 to 1.2, and 0.5 to 3, respectively. It can be observed that on all tested datasets, both  $S^2CAG$  and  $M-S^2CAG$  see a drastic uptick in ACC and reach a plateau afterward when increasing  $\alpha$ . Specifically, when  $\alpha$  is beyond 1.4, 0.9, and 2.0, the ACC scores remain almost invariant on *PubMed*, *DBLP*, and *ArXiv*, respectively. These observations reveal that large  $\alpha$  (especially over 1.0) is conducive for clustering, as it can amplify the feature patterns of far-reaching neighbors in Eq. (6), which are restrained in standard vertex representations calculated in Eq. (3) by limiting  $\alpha$  within (0, 1).

**Varying  $T$ .** Fig. 3 plots the ACC scores of  $S^2CAG$  and  $M-S^2CAG$  when varying order  $T$  from 50 to 200, 1 to 40, and 5 to 35, on *PubMed*, *DBLP*, and *ArXiv*, respectively. Observe that  $S^2CAG$  and  $M-S^2CAG$  experience a rapid improvement in ACC with  $T$  increasing in the beginning. Subsequently, the clustering quality of both of them remains relatively stable on *PubMed* and *DBLP*, but witnesses a sharp performance decline on *ArXiv* when  $T$  exceeds 30. This phenomenon is attributed to the *over-smoothing* [45] and *over-squashing* [2] issues caused by large orders  $T$ . However, on *PubMed*, our methods require an order  $T$  greater than 100 to attain satisfactory performance since vertices inside it are poorly connected.

**Varying  $\gamma$ .** As shown in Fig. 4,  $M-S^2CAG$  achieves the best ACC when  $\gamma$  is around 1.0, which is consistent with the original definition of modularity discussed in Section 5.1. Moreover, it can be observed from Fig. 4 that  $M-S^2CAG$  is highly sensitive to  $\gamma$ , whose performance is considerably inferior when  $\gamma$  is only slightly smaller or greater than 1.0. The reason is that the affinity values  $\hat{Z}_i \cdot \hat{Z}_j \forall v_i, v_j$



in Eq. (12) are small and subtly different due to the normalization. Hence, if  $\gamma$  is large, these affinity values will be masked by  $\gamma \cdot \frac{\omega_i \cdot \omega_j}{\omega_i + \omega_j}$ , and they remain indistinguishable when  $\gamma$  is small.

## 7 CONCLUSION

In this paper, we present two effective and scalable solutions,  $S^2CAG$  and  $M-S^2CAG$ , for SCAG. Under the hood, our proposed methods include (i) a new optimization objective built on an optimized representation model and non-trivial constraints, (ii) fast and theoretically-grounded optimization solvers, and (iii) careful theoretical analyses investigating the rationale underlying  $S^2CAG$  and  $M-S^2CAG$ . Our thorough evaluation results manifest the efficacy of our techniques in addressing the limitations of existing works for vertex clustering over attributed graph datasets of varied volumes.

## ACKNOWLEDGMENTS

Renchi Yang is supported by the NSFC Young Scientists Fund (No. 62302414) and Hong Kong RGC ECS grant (No. 22202623). Xiangyu Ke is supported by the Ningbo Yongjiang Talent Introduction Programme (2022A-237-G) and Zhejiang Province’s “Lingyan” R&D Project under Grant No. 2024C01259.

## REFERENCES

- [1] Esra Akbas and Peixiang Zhao. 2017. Attributed Graph Clustering: an Attribute-aware Graph Embedding Approach. *Proceedings of the IEEE/ACM International Conference on Advances in Social Networks Analysis and Mining* (2017).
- [2] Uri Alon and Eran Yahav. 2021. On the Bottleneck of Graph Neural Networks and its Practical Implications. In *International Conference on Learning Representations*.
- [3] Aritra Bhowmick, Mert Kosan, Zexi Huang, Ambuj Singh, and Sourav Medya. 2024. DGCLUSTER: A Neural Framework for Attributed Graph Clustering via Modularity Maximization. In *Proceedings of the AAAI Conference on Artificial Intelligence*, Vol. 38. 11069–11077.
- [4] Filippo Maria Bianchi, Daniele Grattarola, and Cesare Alippi. 2020. Spectral Clustering with Graph Neural Networks for Graph Pooling. In *Proceedings of the 37th international conference on Machine learning*. ACM, 2729–2738.
- [5] Deyu Bo, Xiao Wang, Chuan Shi, Meiqi Zhu, Emiao Lu, and Peng Cui. 2020. Structural Deep Clustering Network. In *Proceedings of The Web Conference 2020*. Association for Computing Machinery, 1400–1410.
- [6] Aleksandar Bojchevski and Stephan Günnemann. 2017. Deep Gaussian Embedding of Graphs: Unsupervised Inductive Learning via Ranking. *arXiv: Machine Learning* (2017).
- [7] Cécile Bothorel, Juan David Cruz, Matteo Magnani, and Barbora Mícenková. 2015. Clustering attributed graphs: models, measures and methods. *Network Science* 3, 3 (2015), 408–444.
- [8] David Buterez, Ioana Bica, Ifrah Tariq, Helena Andrés-Terré, and Pietro Liò. 2022. CellVGAE: an unsupervised scRNA-seq analysis workflow with graph attention networks. *Bioinformatics* 38, 5 (2022), 1277–1286.
- [9] Jinyu Cai, Jicong Fan, Wenzhong Guo, Shiping Wang, Yunhe Zhang, and Zhao Zhang. 2022. Efficient Deep Embedded Subspace Clustering. *2022 IEEE/CVF Conference on Computer Vision and Pattern Recognition (CVPR)* (2022), 21–30.
- [10] Jie Chen, Hua Mao, Yongsheng Sang, and Zhang Yi. 2014. Subspace clustering using a symmetric low-rank representation. *ArXiv abs/1403.2330* (2014).
- [11] Ming Chen, Zhewei Wei, Zengfeng Huang, Bolin Ding, and Yaliang Li. 2020. Simple and deep graph convolutional networks. In *International conference on machine learning*. PMLR, 1725–1735.
- [12] Yi Cheng and Xiuli Ma. 2022. scGAC: a graph attentional architecture for clustering single-cell RNA-seq data. *Bioinformatics* 38, 8 (2022), 2187–2193.
- [13] René Vidal Chong You, Daniel P. Robinson. 2015. Scalable Sparse Subspace Clustering by Orthogonal Matching Pursuit. *2016 IEEE Conference on Computer Vision and Pattern Recognition (CVPR)* (2015), 3918–3927.
- [14] Petr Chunaev. 2020. Community detection in node-attributed social networks: a survey. *Computer Science Review* 37 (2020), 100286.
- [15] David Combe, Christine Largeron, Elöd Egyed-Zsigmond, and Mathias Géry. 2012. Combining Relations and Text in Scientific Network Clustering. *IEEE/ACM International Conference on Advances in Social Networks Analysis and Mining* (2012), 1248–1253.
- [16] David Combe, Christine Largeron, Mathias Géry, and Elöd Egyed-Zsigmond. 2015. I-Louvain: An Attributed Graph Clustering Method. In *International Symposium on Intelligent Data Analysis*.
- [17] Ganqu Cui, Jie Zhou, Cheng Yang, and Zhiyuan Liu. 2020. Adaptive Graph Encoder for Attributed Graph Embedding. *Proceedings of the 26th ACM SIGKDD International Conference on Knowledge Discovery & Data Mining* (2020).
- [18] Shifei Ding, Benyu Wu, Ling Ding, Xiao Xu, Lili Guo, Hongmei Liao, and Xindong Wu. 2024. Towards Faster Deep Graph Clustering via Efficient Graph Auto-Encoder. *ACM Transactions on Knowledge Discovery from Data* (2024).
- [19] Xiaowen Dong, Dorina Thanou, Pascal Frossard, and Pierre Vandergheynst. 2016. Learning Laplacian matrix in smooth graph signal representations. *IEEE Transactions on Signal Processing* 64, 23 (2016), 6160–6173.
- [20] Amani HB Eissa, Mohamed E El-Sharkawi, and Hoda MO Mokhtar. 2018. Towards recommendation using interest-based communities in attributed social networks. In *Companion Proceedings of the The Web Conference 2018*. 1235–1242.
- [21] Ehsan Elhamifar and René Vidal. 2012. Sparse Subspace Clustering: Algorithm, Theory, and Applications. *IEEE transactions on pattern analysis and machine intelligence* (2012).
- [22] Ehsan Elhamifar and René Vidal. 2013. Sparse subspace clustering: Algorithm, theory, and applications. *IEEE transactions on pattern analysis and machine intelligence* 35, 11 (2013), 2765–2781.
- [23] Issam Falihi, Nistor Grozavu, R. Kanawati, and Younès Bennani. 2017. ANCA : Attributed Network Clustering Algorithm. In *International Workshop on Complex Networks & Their Applications*.
- [24] Jicong Fan. 2021. Large-Scale Subspace Clustering via kFactorization. *SIGKDD Conference on Knowledge Discovery and Data Mining* (2021), 342–352.
- [25] Ky Fan. 1949. On a Theorem of Weyl Concerning Eigenvalues of Linear Transformations I. *PNAS* (1949), 652–5.
- [26] Maryam Fazel. 2002. *Matrix rank minimization with applications*. Ph.D. Dissertation. Stanford University.
- [27] Chakib Fettal, Lazhar Labiod, and Mohamed Nadif. 2022. Efficient Graph Convolution for Joint Node Representation Learning and Clustering. In *Proceedings of the Fifteenth ACM International Conference on Web Search and Data Mining*. Association for Computing Machinery, 289–297.
- [28] Chakib Fettal, Lazhar Labiod, and Mohamed Nadif. 2023. Scalable Attributed-Graph Subspace Clustering. In *Proceedings of the AAAI Conference on Artificial Intelligence*, Vol. 37.
- [29] Hongchang Gao, Feiping Nie, Xuelong Li, and Heng Huang. 2015. Multi-view subspace clustering. In *Proceedings of the IEEE international conference on computer vision*. 4238–4246.
- [30] Johannes Gasteiger, Aleksandar Bojchevski, and Stephan Günnemann. 2018. Predict then Propagate: Graph Neural Networks meet Personalized PageRank. In *International Conference on Learning Representations*.
- [31] Stephan Günnemann, Ines Färber, Sebastian Raubach, and Thomas Seidl. 2013. Spectral subspace clustering for graphs with feature vectors. In *2013 IEEE 13th International Conference on Data Mining*. IEEE, 231–240.
- [32] Nathan Halko, Per-Gunnar Martinsson, and Joel A. Tropp. 2009. Finding Structure with Randomness: Probabilistic Algorithms for Constructing Approximate Matrix Decompositions. *SIAM Rev.* 53 (2009), 217–288.
- [33] Jie Hao and William Zhu. 2022. Deep graph clustering with enhanced feature representations for community detection. *Applied Intelligence* (2022), 1336–1349.
- [34] Kaveh Hassani and Amir Hosein Khas Ahmadi. 2020. Contrastive Multi-View Representation Learning on Graphs. In *International Conference on Machine Learning*.
- [35] Roger A Horn and Charles R Johnson. 2012. *Matrix analysis*. Cambridge university press.
- [36] Weihua Hu, Matthias Fey, Marinka Zitnik, Yuxiao Dong, Hongyu Ren, Bowen Liu, Michele Catasta, and Jure Leskovec. 2020. Open Graph Benchmark: Datasets for Machine Learning on Graphs. *arXiv preprint arXiv:2005.00687* (2020).
- [37] Guangyu Huo, Yong Zhang, Junbin Gao, Boyue Wang, Yongli Hu, and Baocai Yin. 2021. CaEGCN: Cross-Attention Fusion Based Enhanced Graph Convolutional Network for Clustering. *IEEE Transactions on Knowledge and Data Engineering* 35 (2021), 3471–3483.
- [38] Glen Jeh and Jennifer Widom. 2003. Scaling personalized web search. In *Proceedings of the 12th international conference on World Wide Web*. 271–279.
- [39] Pan Ji, T. Zhang, Hongdong Li, Mathieu Salzmann, and Ian D. Reid. 2017. Deep Subspace Clustering Networks. In *Neural Information Processing Systems*.
- [40] Zhao Kang, Zhiping Lin, Xiaofeng Zhu, and Wenbo Xu. 2021. Structured Graph Learning for Scalable Subspace Clustering: From Single View to Multiview. *IEEE Transactions on Cybernetics* 52 (2021), 8976–8986.
- [41] Bhagyashri A Kelkar and Sunil F Rodd. 2019. Subspace clustering—A survey. In *Data Management, Analytics and Innovation: Proceedings of ICDMAI 2018, Volume 1*. Springer, 209–220.
- [42] D. J Ketchen and C. L Shook. 1996. The application of cluster analysis in strategic management research: an analysis and critique. *Strategic management journal* 17, 6 (1996), 441–458.
- [43] Thomas N Kipf and Max Welling. 2022. Semi-Supervised Classification with Graph Convolutional Networks. In *International Conference on Learning Representations*.

- [44] Xinying Lai, Dingming Wu, Christian S Jensen, and Kezhong Lu. 2023. A Re-evaluation of Deep Learning Methods for Attributed Graph Clustering. In *Proceedings of the 32nd ACM International Conference on Information and Knowledge Management*. 1168–1177.
- [45] Qimai Li, Zhichao Han, and Xiao-Ming Wu. 2018. Deeper insights into graph convolutional networks for semi-supervised learning. In *Proceedings of the AAAI conference on artificial intelligence*, Vol. 32.
- [46] Yan Li and Xiaoyun Chen. 2024. Attributed graph subspace clustering with residual compensation guided by adaptive dual manifold regularization. *Expert Systems with Applications* (2024), 124699.
- [47] Yiran Li, Gongyao Guo, Jieming Shi, Renchi Yang, Shiqi Shen, Qing Li, and Jun Luo. 2024. A versatile framework for attributed network clustering via K-nearest neighbor augmentation. *The VLDB Journal* (2024), 1–31.
- [48] Ye Li, Chaofeng Sha, Xin Huang, and Yanchun Zhang. 2018. Community Detection in Attributed Graphs: An Embedding Approach. In *AAAI Conference on Artificial Intelligence*.
- [49] Yiran Li, Renchi Yang, and Jieming Shi. 2023. Efficient and effective attributed hypergraph clustering via k-nearest neighbor augmentation. *Proceedings of the ACM on Management of Data* 1, 2 (2023), 1–23.
- [50] U Liji, Yahui Chai, and Jianrui Chen. 2018. Improved personalized recommendation based on user attributes clustering and score matrix filling. *Computer Standards & Interfaces* 57 (2018), 59–67.
- [51] Chang Liu, Yuwen Yang, Yue Ding, Hongtao Lu, Wenqing Lin, Ziming Wu, and Wendong Bi. 2024. DAG: Deep Adaptive and Generative K-Free Community Detection on Attributed Graphs. In *Proceedings of the ACM SIGKDD international conference on Knowledge discovery and data mining*.
- [52] Guangcan Liu, Zhouchen Lin, and Yong Yu. 2010. Robust Subspace Segmentation by Low-Rank Representation. In *International Conference on Machine Learning*.
- [53] Maoshan Liu, Yan Wang, Jun Sun, and Zhicheng Ji. 2021. Adaptive low-rank kernel block diagonal representation subspace clustering. *Applied Intelligence* 52 (2021), 2301 – 2316.
- [54] Yue Liu, Ke Liang, Jun Xia, Sihang Zhou, Xihong Yang, Xinwang Liu, and Stan Z Li. 2023. Dink-net: Neural clustering on large graphs. In *International Conference on Machine Learning*. PMLR, 21794–21812.
- [55] Yue Liu, Wenxuan Tu, Sihang Zhou, Xinwang Liu, Linxuan Song, Xihong Yang, and En Zhu. 2022. Deep Graph Clustering via Dual Correlation Reduction. In *Proceedings of the AAAI Conference on Artificial Intelligence*, Vol. 36. 7603–7611.
- [56] Yue Liu, Jun Xia, Sihang Zhou, Xihong Yang, Ke Liang, Chenchen Fan, Yan Zhuang, Stan Z Li, Xinwang Liu, and Kunlun He. 2022. A Survey of Deep Graph Clustering: Taxonomy, Challenge, Application, and Open Resource. *arXiv preprint arXiv:2211.12875* (2022).
- [57] László Lovász. 1993. Random walks on graphs. *Combinatorics, Paul erdos is eighty* 2, 1–46 (1993), 4.
- [58] CanYi Lu, Hai Min, ZhongQiu Zhao, Lin Zhu, DeShuang Huang, and Shuicheng Yan. 2012. Robust and Efficient Subspace Segmentation via Least Squares Regression. *Computer Vision-ECCV* 7578 (2012).
- [59] Xiaoqiang Lu, Yulong Wang, and Yuan Yuan. 2013. Graph-Regularized Low-Rank Representation for Destriping of Hyperspectral Images. *IEEE Transactions on Geoscience and Remote Sensing* 51 (2013), 4009–4018.
- [60] Dijun Luo, Feiping Nie, C. Ding, and Heng Huang. 2011. Multi-Subspace Representation and Discovery. In *ECML/PKDD*.
- [61] Xuexiong Luo, Jia Wu, Amin Beheshti, Jian Yang, Xiankun Zhang, Yuan Wang, and Shan Xue. 2022. Comga: Community-aware attributed graph anomaly detection. In *Proceedings of the Fifteenth ACM International Conference on Web Search and Data Mining*. 657–665.
- [62] Yao Ma, Xiaorui Liu, Tong Zhao, Yozen Liu, Jiliang Tang, and Neil Shah. 2020. A Unified View on Graph Neural Networks as Graph Signal Denoising. *Proceedings of the International Conference on Information & Knowledge Management* (2020).
- [63] Zhengrui Ma, Zhao Kang, Guangchun Luo, Ling Tian, and Wenyu Chen. 2020. Towards clustering-friendly representations: Subspace clustering via graph filtering. In *Proceedings of the ACM international conference on multimedia*. 3081–3089.
- [64] Costas Mavromatis and G. Karypis. 2021. Graph InfoClust: Maximizing Coarse-Grain Mutual Information in Graphs. In *PAKDD*.
- [65] Julian McAuley, Christopher Targett, Qinfeng Shi, and Anton van den Hengel. 2015. Image-Based Recommendations on Styles and Substitutes. In *Proceedings of the 38th International ACM SIGIR Conference on Research and Development in Information Retrieval (SIGIR '15)*. Association for Computing Machinery, 43–52.
- [66] Fanrong Meng, Xiaobin Rui, Zhixiao Wang, Yan Xing, and Longbing Cao. 2018. Coupled Node Similarity Learning for Community Detection in Attributed Networks. *Entropy* 20 (2018).
- [67] Waqas Nawaz, Young-Koo Lee, and Sungyoung Lee. 2012. Collaborative Similarity Measure for Intra Graph Clustering. In *DASFAA Workshops*.
- [68] Jennifer Neville, Micah Adler, and David D. Jensen. 2003. Clustering Related Data Using Attribute and Link Information.
- [69] Mark EJ Newman. 2006. Modularity and community structure in networks. *Proceedings of the national academy of sciences* 103, 23 (2006), 8577–8582.
- [70] Krzysztof Nowicki and Tom A. B. Snijders. 2001. Estimation and Prediction for Stochastic Blockstructures. *J. Amer. Statist. Assoc.* 96 (2001), 1077 – 1087.
- [71] Lance Parsons, Ehtesham Haque, and Huan Liu. 2004. Subspace clustering for high dimensional data: a review. *ACM SIGKDD Explorations Newsletter* (2004), 90–105.
- [72] Vishal M. Patel and René Vidal. 2014. Kernel sparse subspace clustering. *2014 IEEE International Conference on Image Processing (ICIP)* (2014), 2849–2853.
- [73] Xi Peng, Jiashi Feng, Joey Tianyi Zhou, Yingjie Lei, and Shuicheng Yan. 2020. Deep subspace clustering. *IEEE transactions on neural networks and learning systems* 31, 12 (2020), 5509–5521.
- [74] Wentao Qu, Xianchao Xiu, Huangyue Chen, and Lingchen Kong. 2023. A survey on high-dimensional subspace clustering. *Mathematics* 11, 2 (2023), 436.
- [75] Yiye Ruan, David Fuhry, and Srinivasan Parthasarathy. 2012. Efficient community detection in large networks using content and links. *Proceedings of the 22nd international conference on World Wide Web* (2012).
- [76] Yousef Saad. 2011. *Numerical methods for large eigenvalue problems: revised edition*. SIAM.
- [77] Peter H. Schönemann. 1966. A generalized solution of the orthogonal procrustes problem. *Psychometrika* 31 (1966), 1–10.
- [78] Prithviraj Sen, Galileo Namata, Mustafa Bilgic, Lise Getoor, Brian Gallagher, and Tina Eliassi-Rad. 2008. Collective Classification in Network Data. *AI Mag.* 29, 3 (sep 2008), 93–106.
- [79] Shi. 2003. Multiclass spectral clustering. In *Proceedings ninth IEEE international conference on computer vision*. IEEE, 313–319.
- [80] Jianbo Shi and Jitendra Malik. 2000. Normalized cuts and image segmentation. *IEEE Transactions on pattern analysis and machine intelligence* (2000), 888–905.
- [81] Karsten Steinhaeuser and N. Chawla. 2008. Community Detection in a Large Real-World Social Network.
- [82] Yao Sui, Guanghui Wang, and Li Zhang. 2019. Sparse subspace clustering via low-rank structure propagation. *Pattern Recognition* 95 (2019), 261–271.
- [83] Jie Tang, Jing Zhang, Limin Yao, Juanzi Li, Li Zhang, and Zhong Su. 2008. Arnetminer: extraction and mining of academic social networks. In *Proceedings of the ACM SIGKDD international conference on Knowledge discovery and data mining*. 990–998.
- [84] Anton Tsitsulin, John Palowitch, Bryan Perozzi, and Emmanuel Müller. 2023. Graph clustering with graph neural networks. *Journal of Machine Learning Research* 24, 127 (2023), 1–21.
- [85] Wenxuan Tu, Sihang Zhou, Xinwang Liu, Xifeng Guo, Zhiping Cai, En Zhu, and Jieren Cheng. 2020. Deep Fusion Clustering Network. *ArXiv abs/2012.09600* (2020).
- [86] René Vidal. 2011. Subspace clustering. *IEEE Signal Processing Magazine* 28, 2 (2011), 52–68.
- [87] Ulrike Von Luxburg. 2007. A tutorial on spectral clustering. *Statistics and computing* 17 (2007), 395–416.
- [88] Chun Wang, Shirui Pan, Ruiqi Hu, Guodong Long, Jing Jiang, and Chengqi Zhang. 2019. Attributed graph clustering: a deep attentional embedding approach. In *Proceedings of the 28th International Joint Conference on Artificial Intelligence*. 3670–3676.
- [89] Yu-Xiang Wang, Huan Xu, and Chenlei Leng. 2013. Provable subspace clustering: When LRR meets SSC. *Advances in Neural Information Processing Systems* (2013).
- [90] Lai Wei, Zhengwei Chen, Jun Yin, Changming Zhu, Rigui Zhou, and Jin Liu. 2023. Adaptive graph convolutional subspace clustering. In *Proceedings of the IEEE/CVF Conference on Computer Vision and Pattern Recognition*. 6262–6271.
- [91] Hui Xia, Shu shu Shao, Chun qiang Hu, Rui Zhang, Tie Qiu, and Fu Xiao. 2023. Robust Clustering Model Based on Attention Mechanism and Graph Convolutional Network. *IEEE Transactions on Knowledge and Data Engineering* 35 (2023), 5203–5215.
- [92] Wang Xiao, Ji Houye, Shi Chuan, Wang Bai, Cui Peng, Yu P., and Ye Yanfang. 2019. Heterogeneous Graph Attention Network. *WWW* (2019).
- [93] Zhiqiang Xu, Yiping Ke, Yi Wang, Hong Cheng, and James Cheng. 2012. A model-based approach to attributed graph clustering. *Proceedings of the 2012 ACM SIGMOD International Conference on Management of Data* (2012).
- [94] Cheng Yang, Zhiyuan Liu, Deli Zhao, Maosong Sun, and Edward Y. Chang. 2015. Network representation learning with rich text information. In *Proceedings of the 24th International Conference on Artificial Intelligence (Buenos Aires, Argentina) (IJCAI'15)*. AAAI Press, 2111–2117.
- [95] Renchi Yang and Jieming Shi. 2024. Efficient High-Quality Clustering for Large Bipartite Graphs. *Proceedings of the ACM on Management of Data* (2024), 1–27.
- [96] Renchi Yang, Jieming Shi, Xiaokui Xiao, Yin Yang, Sourav S Bhowmick, and Juncheng Liu. 2023. PANE: scalable and effective attributed network embedding. *The VLDB Journal* 32, 6 (2023), 1237–1262.
- [97] Renchi Yang, Jieming Shi, Yin Yang, Keke Huang, Shiqi Zhang, and Xiaokui Xiao. 2021. Effective and scalable clustering on massive attributed graphs. In *Proceedings of the Web Conference 2021*. 3675–3687.
- [98] Renchi Yang, Yidu Wu, Xiaoyang Lin, Qichen Wang, Tsz Nam Chan, and Jieming Shi. 2024. Effective Clustering on Large Attributed Bipartite Graphs. In *Proceedings of the 30th ACM SIGKDD Conference on Knowledge Discovery and Data Mining*. 3782–3793.

- [99] Tianbao Yang, Rong Jin, Yun Chi, and Shenghuo Zhu. 2014. Combining Link and Content for Community Detection. In *Encyclopedia of Social Network Analysis and Mining*.
- [100] Xihong Yang, Yue Liu, Sihang Zhou, Siwei Wang, Wenxuan Tu, Qun Zheng, Xinwang Liu, Liming Fang, and En Zhu. 2023. Cluster-guided Contrastive Graph Clustering Network. *ArXiv abs/2301.01098* (2023).
- [101] Hugo Zanghi, Stevonn Volant, and Christophe Ambroise. 2009. Clustering based on random graph model embedding vertex features. *Pattern Recognit. Lett.* 31 (2009), 830–836.
- [102] Changqing Zhang, Huazhu Fu, Qinghua Hu, Xiaochun Cao, Yuan Xie, Dacheng Tao, and Dong Xu. 2018. Generalized latent multi-view subspace clustering. *IEEE transactions on pattern analysis and machine intelligence* 42, 1 (2018), 86–99.
- [103] Han Zhao, Xu Yang, Zhenru Wang, Erkun Yang, and Cheng Deng. 2021. Graph Debaised Contrastive Learning with Joint Representation Clustering. In *International Joint Conference on Artificial Intelligence*.
- [104] Qiqi Zhao, Huifang Ma, Lijun Guo, and Zhixin Li. 2022. Hierarchical attention network for attributed community detection of joint representation. *Neural Computing and Applications* 34 (2022), 5587–5601.
- [105] Lei Zhou, Xiao Bai, Dong Wang, Xianglong Liu, Jun Zhou, and Edwin R. Hancock. 2019. Latent Distribution Preserving Deep Subspace Clustering. In *International Joint Conference on Artificial Intelligence*.
- [106] Pan Zhou, Yunqing Hou, and Jiashi Feng. 2018. Deep Adversarial Subspace Clustering. *2018 IEEE/CVF Conference on Computer Vision and Pattern Recognition* (2018), 1596–1604.
- [107] Xinchuang Zhou, Lingtao Su, Xiangju Li, Zhongying Zhao, and C. Li. 2022. Community detection based on unsupervised attributed network embedding. *Expert Syst. Appl.* 213 (2022), 118937.
- [108] Hao Zhu and Piotr Koniusz. 2021. Simple Spectral Graph Convolution. In *International Conference on Learning Representations*.
- [109] Jiong Zhu, Yujun Yan, Lingxiao Zhao, Mark Heimann, Leman Akoglu, and Danai Koutra. 2020. Beyond homophily in graph neural networks: Current limitations and effective designs. *Advances in neural information processing systems* 33 (2020), 7793–7804.
- [110] Meiqi Zhu, Xiao Wang, Chuan Shi, Houye Ji, and Peng Cui. 2021. Interpreting and Unifying Graph Neural Networks with An Optimization Framework. *Proceedings of the Web Conference 2021* (2021).

## A ALGORITHMIC DETAILS

### A.1 PowerMethod

Algo. 3 displays the pseudo-code of PowerMethod for computing  $Z$  defined in Eq. (6) in an iterative manner. Specifically, after taking as inputs matrices  $\hat{P}$ ,  $\hat{X}$ , an integer  $T$ , and decay factor  $\alpha$ , Algo. 3 initializes  $Z$  as  $\frac{1-\alpha}{1-\alpha^{T+1}} \cdot \hat{X}$ . Later, S<sup>2</sup>CAG starts  $T$  rounds of matrix multiplications and each round updates  $Z$  by

$$Z \leftarrow \alpha \cdot \hat{P}Z + \frac{1-\alpha}{1-\alpha^{T+1}} \cdot \hat{X}, \quad (17)$$

and returns the  $Z$  at the end of  $T$ -th iteration as the output.

---

#### Algorithm 3: PowerMethod

---

**Input:** Matrices  $\hat{P}$ ,  $\hat{X}$ , order  $T$ , decay factor  $\alpha$

**Output:** NSR  $Z$

- 1  $Z \leftarrow \frac{1-\alpha}{1-\alpha^{T+1}} \cdot \hat{X}$ ;
  - 2 **for**  $t \leftarrow 1$  **to**  $T$  **do**
  - 3      $Z \leftarrow \alpha \cdot \hat{P}Z + \frac{1-\alpha}{1-\alpha^{T+1}} \cdot \hat{X}$ ;
- 

Since  $\hat{P}$  is a sparse matrix containing  $m$  non-zero entries, the sparse matrix multiplication  $\hat{P}Z$  can be done in  $O(dm)$  time. The total cost is hence  $O(Tdm)$  for  $T$  iterations.

### A.2 Complexity Analyses

**S<sup>2</sup>CAG.** First, we consider the naive method at Lines 2-3 of Algo. 1. According to Section A.1, the construction of NSR  $Z$  at Line 2 takes

$O(Tdm)$ . As for Line 3, our implementation of the randomized SVD algorithm [32] involves  $2 \cdot (\tau + 1) \cdot (k + o)dn + 3 \cdot (k + o)^2n$  matrix operations. In sum, the empirical cost can be estimated by

$$f_{\text{naive}}(\mathcal{G}, k, \tau, T) = Tdm + 2(\tau + 1) \cdot (k + o)dn + 3(k + o)^2n.$$

The asymptotic complexity can be simplified as  $O(Tdm + k\tau dn)$  since the oversampling parameter  $o$  can be regarded as a constant.

The major cost of the integrated method lies at Lines 6-13 of Algo. 1. As per Section A.1, for each of the  $\tau$  iterations, both Lines 7 and 8 incur  $T(k + o)m$  operations when executing PowerMethod, while Lines 7 and 9 need  $(k + o)dn$  operations for computing  $\hat{X}R$  and  $\hat{X}^\top H$ . Similarly, we can analyze that the cost of Lines 10 and 12 is  $2T(k + o)m + 2(k + o)dn$ . To sum up, Lines 6-9, 10, and 12 together involve  $2(\tau + 1) \cdot (k + o) \cdot (dn + Tm)$  operations in total. Since the QR decomposition and SVD are applied to  $n \times (k + o)$  and  $(k + o) \times n$  matrices, respectively, both their runtime can be bounded by  $O((k + o)^2n)$ . The matrix multiplication in Eq. (10) also requires  $O((k + o)^2n)$  operations. Overall, the estimated computational cost of the integrated method can be calculated by

$$f_{\text{integr}}(\mathcal{G}, k, \tau, T) = 2(\tau + 1) \cdot (k + o) \cdot (dn + Tkm) + 3(k + o)^2n, \quad (18)$$

which leads to a theoretical time complexity of  $O(\tau(kdn + Tm))$  when regarding  $o$  as a constant. By adaptively selecting these two approaches to run, the runtime complexity of S<sup>2</sup>CAG is guaranteed to be bounded by  $O(k\tau dn + \min\{\tau Tm, Tdm\})$ .

**M-S<sup>2</sup>CAG.** Line 1 invokes Algo. 3 with  $T$  iterations, and hence, takes  $O(Tdm)$  time. The computation of  $\hat{Z}$  at Line 2 can be done in  $O(dn)$  time since we can first calculate vector  $z = \sum_{v_j \in \mathcal{V}} Z_j$ , followed by a normalization operation  $\frac{Z_i}{Z_i \cdot z^\top}$  for each  $v_i \in \mathcal{V}$ . Similarly, we can compute  $\omega$  by setting  $\omega_i = \hat{Z}_i \cdot \hat{z}^\top$  for each vertex  $v_i \in \mathcal{V}$ , where  $\hat{z}$  is a sum of all row vectors in  $\hat{Z}$ , i.e.,  $\hat{z} = \sum_{v_j \in \mathcal{V}} \hat{Z}_j$ . The cost is also  $O(dn)$ . Both Lines 4 and 7 apply a QR decomposition of an  $n \times k$  matrix, requiring  $O(k^2n)$  time. Note that Eq. (15) can be computed in  $O(kdn)$  via re-ordered matrix multiplications. Considering all the  $\tau$  iterations, the total cost for updating  $H$  and  $Q$  is then  $O(k\tau dn)$ . Overall, the runtime complexity of M-S<sup>2</sup>CAG is bounded by  $O(Tdm + k\tau dn)$ .

**Table 4: Statistics for  $\beta_\ell \forall v_\ell \in \mathcal{V}$ .**

	ACM	Wiki	CiteSeer	Photo	DBLP
Mean	0.996	0.986	0.99	0.967	0.951
Variance	0.004	0.013	0.009	0.031	0.044

**Table 5: Statistics for  $\sum_{v_j \in \mathcal{V}} Z_i \cdot Z_j^\top \forall v_i \in \mathcal{V}$ .**

	ACM	Wiki	CiteSeer	Photo	DBLP
Mean	0.64	1.88	0.63	1.76	0.788
Variance	9.2e-4	0.04	2.62e-3	0.019	3.11e-3

### A.3 Stochasticity Analysis of $ZZ^\top$

For ease of exposition, for any vertex  $v_\ell \in \mathcal{V}$ , we first define

$$\beta_\ell = \sum_{v_h \in \mathcal{V}} \hat{X}_\ell \cdot \hat{X}_h^\top \text{ and } \pi_\ell = \sum_{v_h \in \mathcal{V}} \sum_{t=0}^T \frac{\alpha^t}{\sum_{l=0}^T \alpha^l} \hat{P}_{h,\ell}^t.$$

LEMMA A.1.  $\forall v_i \in \mathcal{V}, \min_{v_\ell \in \mathcal{V}} \beta_\ell \cdot \pi_\ell \leq \sum_{v_j \in \mathcal{V}} Z_i Z_j^\top \leq \max_{v_\ell \in \mathcal{V}} \beta_\ell \cdot \pi_\ell$ .

Lemma A.1 provides upper and lower bounds for the sum of entries in each row of  $\mathbf{Z}\mathbf{Z}^\top$ , which are dependent on the maximums and minimums of  $\beta_\ell$  and  $\pi_\ell$ . In what follows, we show that the variables in  $\{\beta_\ell | v_\ell \in \mathcal{V}\}$  and  $\{\pi_\ell | v_\ell \in \mathcal{V}\}$  are dispersed in a narrow value range with low variances, making  $\sum_{v_j \in \mathcal{V}} \mathbf{Z}_i \mathbf{Z}_j^\top \forall v_i \in \mathcal{V}$  nearly identical.

LEMMA A.2.  $\sum_{v_\ell \in \mathcal{V}} \beta_\ell = n$ .

Theoretically, the above lemma states that the average value of  $\beta_\ell \forall v_\ell \in \mathcal{V}$  is 1, which accords with its empirical means reported in Table 4. Additionally, the variances of  $\beta_\ell \forall v_\ell \in \mathcal{V}$  on the five datasets are almost negligible, implying that  $\min_{v_\ell} \beta_\ell \approx \max_{v_\ell} \beta_\ell$ .

LEMMA A.3. For any vertex  $v_\ell$ , the following inequality

$$\frac{\hat{d}(v_\ell)}{\max_{v_h \in \mathcal{N}_{v_\ell} \cap \{v_\ell\}} \hat{d}(v_h)} \leq \pi_\ell \leq \frac{\hat{d}(v_\ell)}{\min_{v_h \in \mathcal{N}_{v_\ell} \cap \{v_\ell\}} \hat{d}(v_h)},$$

holds, where  $\hat{d}(v_h) = \sum_{v_j \in \mathcal{V}} \hat{\mathbf{A}}_{h,j}$  and  $\hat{d}(v_\ell) = \sum_{v_j \in \mathcal{V}} \hat{\mathbf{A}}_{\ell,j}$ .

Our task thus turns to bound  $\pi_\ell \forall v_\ell \in \mathcal{V}$ , which is done in Lemma A.3. Since  $\hat{\mathbf{A}}$  is normalized, the values in  $\{\hat{d}(v_\ell) | v_\ell \in \mathcal{V}\}$  has a little variation, namely  $\min_{v_\ell} \pi_\ell$  and  $\max_{v_\ell} \pi_\ell$  are close. As a consequence, the row sums  $\sum_{v_j \in \mathcal{V}} \mathbf{Z}_i \cdot \mathbf{Z}_j^\top \forall v_i \in \mathcal{V}$  are closely aligned, which can be corroborated by our empirical observations on each dataset from Table 5 and indicates that  $\mathbf{Z}\mathbf{Z}^\top$  is nearly a scaled stochastic matrix.

## B ADDITIONAL EXPERIMENTS

Table 6 lists the detailed settings of parameters used in  $\mathbf{S}^2\text{CAG}$  and  $\mathbf{M}\text{-}\mathbf{S}^2\text{CAG}$ , including decay factor  $\alpha$ , order  $T$ , the number of iterations  $\tau$ , and weight  $\gamma$ .

Table 6: Parameter Settings in  $\mathbf{S}^2\text{CAG}/\mathbf{M}\text{-}\mathbf{S}^2\text{CAG}$ .

	ACM	Wiki	CiteSeer	Photo	DBLP	PubMed	Cora	ArXiv
$\alpha$	0.8	1.7	0.8	1.5	0.9	1.8	0.9/1.4	1.4/2.5
$T$	15	6/12	60/40	9	10	175	20/7	30
$\tau$	7/50	7/50	7/100	7/50	7/50	7/50	7/100	4/50
$\gamma$	1	0.9	0.9	1	1	1	1	1

### B.1 Clustering Visualization

We visually compare the clustering results output by  $\mathbf{S}^2\text{CAG}$  and  $\text{SAGSC}$  against the ground truth on *Wiki*, *ACM*, and *PubMed* datasets. Specifically, for each of them, we run the well-known Fruchterman-Reingold force-directed algorithm to draw the layout of the graph, wherein vertices are colored as per their respective cluster labels (true ones or predicted ones).

Fig. 6, 5, 7 display the visualization results of the ground truth,  $\mathbf{S}^2\text{CAG}$  and  $\text{SAGSC}$  on *Wiki*, *ACM*, and *PubMed*, respectively. The major differences between the predicted results and the ground truth are highlighted in the rectangles. It can be observed that compared to  $\text{SAGSC}$ , the vertices in the highlighted areas are colored (i.e., assign cluster labels to vertices) in a way more similar to the ground truth by  $\mathbf{S}^2\text{CAG}$ , which is consistent with the fact that  $\mathbf{S}^2\text{CAG}$  enjoys higher clustering accuracy. For example, in Fig. 7, in the three rectangles, most of the vertices are mistakenly colored in green by  $\text{SAGSC}$ , whereas our  $\mathbf{S}^2\text{CAG}$  can color them in red and blue correctly. Accordingly, as reported in Table 3, on *PubMed*,  $\mathbf{S}^2\text{CAG}$  outperforms  $\text{SAGSC}$  remarkably by a substantial margin of 4.2%, 3.6%, and 7.8% for ACC, NMI, and ARI, respectively.

## C THEORETICAL PROOFS

**Proof of Lemma 4.1.** Suppose that  $\Omega^\top \Omega = \mathbf{I}$ . Then,

$$\begin{aligned} \|\Omega \mathbf{M} - \mathbf{N}\|_F^2 &= \langle \Omega \mathbf{M} - \mathbf{N}, \Omega \mathbf{M} - \mathbf{N} \rangle_F \\ &= \|\Omega \mathbf{M}\|_F^2 + \|\mathbf{N}\|_F^2 - 2\langle \Omega \mathbf{M}, \mathbf{N} \rangle_F \\ &= \|\mathbf{M}\|_F^2 + \|\mathbf{N}\|_F^2 - 2\langle \Omega \mathbf{M}, \mathbf{N} \rangle_F \\ &= \|\mathbf{M}\|_F^2 + \|\mathbf{N}\|_F^2 - 2\text{trace}(\mathbf{N}\mathbf{M}^\top \Omega^\top). \end{aligned}$$

Hence, the minimization of  $\|\Omega \mathbf{M} - \mathbf{N}\|_F^2$  is equivalent to maximizing  $\text{trace}(\mathbf{N}\mathbf{M}^\top \Omega^\top)$ . Let  $\mathbf{U}\Sigma\mathbf{V}^\top$  be the full SVD of  $\mathbf{N}\mathbf{M}^\top$ . Let  $\mathbf{T} = \mathbf{U}^\top \Omega \mathbf{V}$ , which is an orthogonal matrix since  $\mathbf{T}^\top \mathbf{T} = \mathbf{I}$ . This further implies that  $-1 \leq T_{i,i} \leq 1 \forall i \in [1, n]$ . Next, using the properties of matrix trace, we derive

$$\begin{aligned} \text{trace}(\mathbf{N}\mathbf{M}^\top \Omega^\top) &= \text{trace}(\mathbf{U}\Sigma\mathbf{V}^\top \Omega^\top) = \text{trace}(\mathbf{U}^\top \Omega \mathbf{V}\Sigma) \\ &= \text{trace}(\mathbf{T}\Sigma) = \sum_{i=1}^n T_{i,i} \cdot \Sigma_{i,i} \leq \sum_{i=1}^n \Sigma_{i,i}, \end{aligned}$$

meaning that the trace  $\text{trace}(\mathbf{N}\mathbf{M}^\top \Omega^\top)$  is maximized when  $\mathbf{T} = \mathbf{I}$ . To achieve this, we need to find a rank- $k$  matrix  $\Omega$  minimizing

$$\|\mathbf{T} - \mathbf{I}\|_F^2 = \|\mathbf{U}^\top \Omega \mathbf{V} - \mathbf{I}\|_F^2.$$

Since the columns of  $\mathbf{U}$  (resp.  $\mathbf{V}$ ) are singular vectors that are orthonormal, the problem can be rewritten as

$$\min_{\text{rank}(\Omega)=k} \|\Omega - \mathbf{U}\mathbf{V}^\top\|_F^2,$$

which is a classic *low-rank approximation* problem. By Eckart–Young theorem [35], the solution can be derived through a  $k$ -truncated SVD over  $\mathbf{U}\mathbf{V}^\top$ , implying that  $\Omega = \mathbf{U}^{(k)}\mathbf{V}^{(k)\top}$ .  $\square$

**Proof of Lemma 4.2.**

**THEOREM C.1** ([35]). Let  $\mathbf{M}$  be an  $n \times n$  real symmetric matrix. Let columns in  $\mathbf{\Gamma}$ ,  $\mathbf{Y}$ , and  $\mathbf{\Psi}$  be the left singular vectors, right singular vectors, and eigenvectors, respectively. Diagonal matrices  $\Phi$  and  $\Lambda$  consist of the singular values and eigenvalues of  $\mathbf{M}$  at their diagonal entries, respectively. Then,  $\Gamma_{\cdot,i} = \Psi_{\cdot,i}$ ,  $\mathbf{Y}_{\cdot,i} = \mathbf{\Psi}_{\cdot,i} \cdot \text{sign}(\Lambda_{i,i})$ , and  $\Phi_{i,i} = |\Lambda_{i,i}|$  hold for  $1 \leq i \leq n$ , where  $\text{sign}(\cdot)$  stands for the sign function, i.e.,  $\text{sign}(x) = 1$  if  $x > 0$ ,  $\text{sign}(x) = 0$  if  $x = 0$ , and  $\text{sign}(x) = -1$  if  $x < 0$ .

Let  $\mathbf{U}^{(k)}$  (resp.  $\mathbf{V}^{(k)}$ ) contain the top- $k$  left (resp. right) singular vectors of  $\mathbf{Z}\mathbf{Z}^\top$ . Next, we prove that  $\mathbf{U}^{(k)} = \mathbf{V}^{(k)}$  and it is the top- $k$  left singular vectors of  $\mathbf{Z}$ . Let the columns in  $\mathbf{U}^*$ ,  $\mathbf{V}^*$ , and the diagonal entries in  $\Sigma^*$  be the left singular vectors, right singular vectors, and singular values of  $\mathbf{Z}$ , respectively. Using the relation of SVD to eigendecomposition [35], the columns of  $\mathbf{U}^*$  are eigenvectors of  $\mathbf{Z}\mathbf{Z}^\top$  and the diagonal elements of  $\Sigma^*$  are the square roots of the eigenvalues of  $\mathbf{Z}\mathbf{Z}^\top$ . In other words,  $\mathbf{U}^* \Sigma^{*2} \mathbf{U}^{*\top}$  is the eigendecomposition of  $\mathbf{Z}\mathbf{Z}^\top$ . Further, according to Theorem C.1,  $\mathbf{U}$  is equal to the eigenvectors of  $\mathbf{Z}\mathbf{Z}^\top$ , and thus,  $\mathbf{U} = \mathbf{U}^*$ .

Note that singular values in  $\Sigma^*$  are non-negative. The top- $k$  singular vectors in  $\mathbf{U}^*$  of  $\mathbf{Z}$  are then exactly the  $k$ -largest eigenvectors of  $\mathbf{Z}\mathbf{Z}^\top$  since its eigendecomposition is  $\mathbf{U}^* \Sigma^{*2} \mathbf{U}^{*\top}$ . By Theorem C.1 and the non-negativity of  $\Sigma^{*2}$ , the eigenvalues  $\Sigma^{*2}$  of  $\mathbf{Z}\mathbf{Z}^\top$  are the same as its singular values  $\Sigma$  and  $\mathbf{V} = \mathbf{V}^*$ . Accordingly,  $\mathbf{U}^* \Sigma^{*2} \mathbf{U}^{*\top}$  is

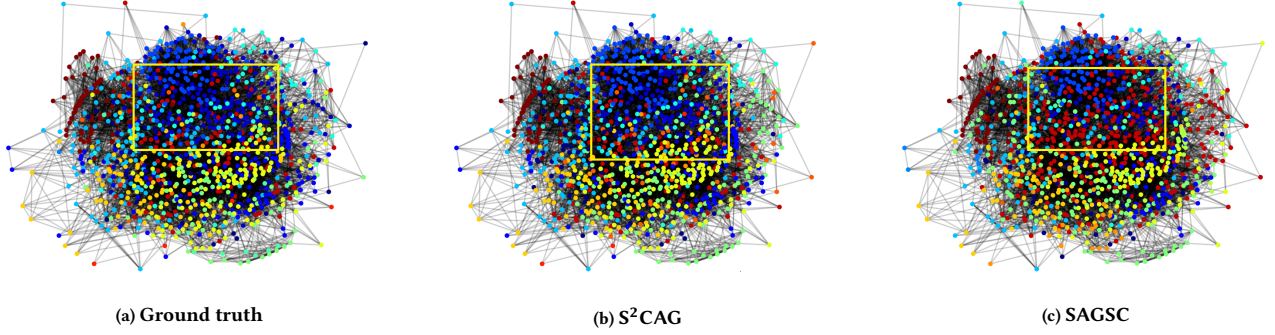


Figure 5: Visualizations on Wiki.

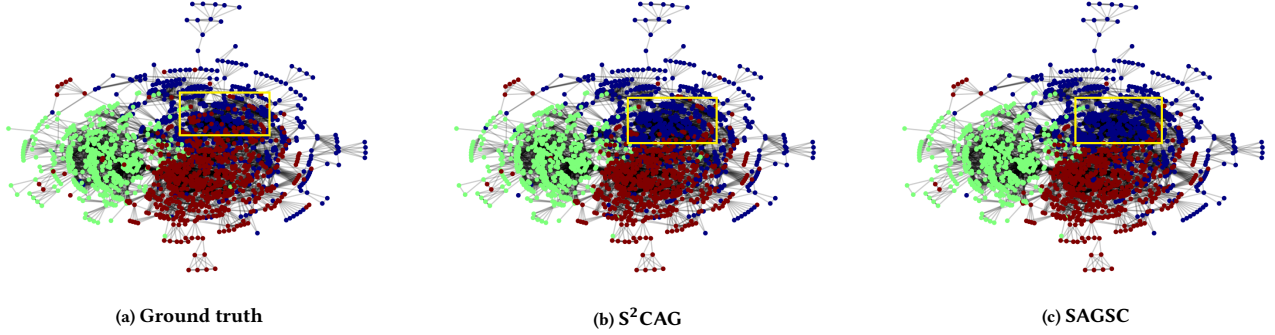


Figure 6: Visualizations on ACM.

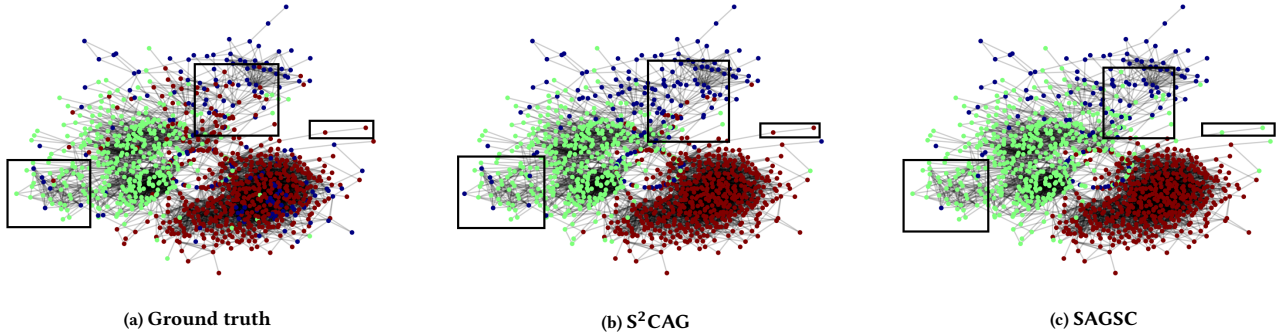


Figure 7: Visualizations on PubMed.

the full SVD of  $ZZ^\top$ , namely,  $U^{(k)} = V^{(k)}$  is the top- $k$  left singular vectors of  $Z$ , which proves the lemma.  $\square$

**Proof of Lemma 4.3.** Recall that the columns of  $U^{(k)} \in \mathbb{R}^{n \times k}$  are the top- $k$  left singular vectors of  $Z$ . Hence, the columns in  $U^{(k)}$  are orthonormal. Consider any column  $U^{(k)}_{:,i}$  of  $U^{(k)} \forall 1 \leq i \leq k$ . We have

$$U^{(k)} U^{(k)\top} \cdot U^{(k)}_{:,i} = U^{(k)} e_i = U^{(k)}_{:,i},$$

where  $e_i \in \mathbb{R}^k$  stands for a column vector with value 1 at the  $i$ -th position and 0 elsewhere. The above equation implies that columns of  $U^{(k)}$  are all eigenvectors of  $U^{(k)} U^{(k)\top}$  whose corresponding eigenvalues are 1.

By the definition,  $U^{(k)} U^{(k)\top}$  is a rank- $k$  projection matrix onto the subspace spanned by the columns of  $U^{(k)}$ , whose eigenvalues

are either 0 or 1. Since its rank is  $k$ , i.e., the sum of all eigenvalues is  $k$ ,  $U^{(k)} U^{(k)\top}$  has  $k$  eigenvectors corresponding to eigenvalue 1 and other eigenvectors not in the span of  $U_k$  correspond to the eigenvalue 0. Consequently, we can conclude that the columns of  $U^{(k)}$  are the  $k$ -largest eigenvectors of  $U^{(k)} U^{(k)\top}$  and the lemma is proved.  $\square$

**Proof of Theorem 4.4.** Let  $R^{(0)}$  be the matrix  $R$  generated at Line 5. Consider any iteration of Lines 7-9 in Algo. 1. Based on Eq. (6), the output  $H$  at Line 7 is  $\sum_{t=0}^T \frac{(1-\alpha)\alpha^t}{1-\alpha^{T+1}} \hat{P}^t \hat{X} R = ZR$  and Line 8 returns

$$\sum_{t=0}^T \frac{(1-\alpha)\alpha^t}{1-\alpha^{T+1}} \hat{P}^{\top t} H = \sum_{t=0}^T \frac{(1-\alpha)\alpha^t}{1-\alpha^{T+1}} \hat{P}^{\top t} ZR.$$

Accordingly, Line 9 yields

$$\mathbf{R} = \hat{\mathbf{X}}^\top \mathbf{H} = \hat{\mathbf{X}}^\top \sum_{t=0}^T \frac{(1-\alpha)\alpha^t}{1-\alpha^{T+1}} \hat{\mathbf{P}}^\top{}^t \mathbf{Z}\mathbf{R} = \mathbf{Z}^\top \mathbf{Z}\mathbf{R}.$$

After repeating the above matrix multiplications for  $\tau$  times, we have  $\mathbf{R} = (\mathbf{Z}^\top \mathbf{Z})^\tau \mathbf{R}^{(0)}$  at the end of  $\tau$ -th iteration. Line 10 further derives

$$\mathbf{H} = \sum_{t=0}^T \frac{(1-\alpha)\alpha^t}{1-\alpha^{T+1}} \hat{\mathbf{P}}^t \cdot \hat{\mathbf{X}}\mathbf{R} = \mathbf{Z} \cdot (\mathbf{Z}^\top \mathbf{Z})^\tau \mathbf{R}^{(0)} = (\mathbf{Z}\mathbf{Z}^\top)^\tau \mathbf{Z}\mathbf{R}^{(0)}.$$

$\mathbf{B}$  is calculated as at Line 12, which equals  $\sum_{t=0}^T \frac{(1-\alpha)\alpha^t}{1-\alpha^{T+1}} \hat{\mathbf{P}}^\top{}^t \mathbf{Q}$  and yields

$$\mathbf{B}^\top \hat{\mathbf{X}} = \mathbf{Q}^\top \sum_{t=0}^T \frac{(1-\alpha)\alpha^t}{1-\alpha^{T+1}} \hat{\mathbf{P}}^t \hat{\mathbf{X}} = \mathbf{Z}\hat{\mathbf{X}}$$

. Let  $\Gamma \Sigma \mathbf{V}^\top$  be the SVD of  $\mathbf{B}^\top \hat{\mathbf{X}}$ . According to Theorem 1.2 in [32], we have

$$\|\mathbf{Z} - \mathbf{Y}'\Sigma\mathbf{V}^\top\| \leq \left(1 + 4\sqrt{\frac{2\min\{n, d\}}{(k+o)/2-1}}\right)^{\frac{1}{2\tau+1}} \cdot \sigma_{(k+o)/2+1},$$

where  $\sigma_{(k+o)/2+1}$  signifies the  $((k+o)/2+1)$ -th largest singular value of  $\mathbf{Z}$ . In sum, the columns in  $\mathbf{Y}$  are the approximate top- $(k+o)$  left singular vectors of  $\mathbf{Z}$ .  $\square$

**Proof of Lemma 4.5.** Using Ky Fan's trace maximization principle [25], the optimal solution to the following trace maximization problem  $\max_{\mathbf{Y} \in \mathbb{R}^{n \times k}} \text{trace}(\mathbf{Y}^\top \mathbf{Z}\mathbf{Z}^\top \mathbf{Y})$  subject to  $\mathbf{Y}^\top \mathbf{Y} = \mathbf{I}$  is the  $k$ -largest eigenvectors of  $\mathbf{Z}\mathbf{Z}^\top$ . Since  $\mathbf{Y}$  is the top- $k$  left singular vectors of  $\mathbf{Z}$  and  $\mathbf{Z}\mathbf{Z}^\top$  is a symmetric matrix, Theorem C.1 states that  $\mathbf{Y}$  is also the  $k$ -largest eigenvectors of  $\mathbf{Z}\mathbf{Z}^\top$ . The lemma is proved.  $\square$

**Proof of Lemma 4.6.** Since  $\beta \cdot \mathbf{W}$  is a stochastic matrix, then  $\frac{\mathbf{I}}{\beta} - \mathbf{W}$  is the Laplacian of  $\hat{\mathcal{G}}$ . For any row vector  $\mathbf{x} \in \mathbb{R}^n$ , it is easy to verify that

$$\mathbf{x}^\top \left(\frac{\mathbf{I}}{\beta} - \mathbf{W}\right) \mathbf{x} = \frac{1}{2} \sum_{v_i, v_j \in \mathcal{V}} \mathbf{W}_{i,j} \cdot (\mathbf{x}_i - \mathbf{x}_j)^2.$$

Let  $\{C_1, C_2, \dots, C_k\}$  be the clusters corresponding to the VCA matrix  $\mathbf{C}$ . By the definition of  $\mathbf{C}$  and its orthogonality property  $\mathbf{C}^\top \mathbf{C} = \mathbf{I}$ , we deduce

$$\begin{aligned} \text{trace}(\mathbf{C}^\top \mathbf{W}\mathbf{C}) &= k - \text{trace}\left(\mathbf{C}^\top \left(\frac{\mathbf{I}}{\beta} - \mathbf{W}\right) \mathbf{C}\right) \\ &= k - \frac{1}{2} \sum_{\ell=1}^d \sum_{v_i, v_j \in \mathcal{V}} \mathbf{W}_{i,j} \cdot (\mathbf{C}_{i,\ell} - \mathbf{C}_{j,\ell})^2 \\ &= k - \frac{1}{2} \sum_{\ell=1}^d \sum_{v_i \in C_\ell, v_j \notin C_\ell} \frac{\mathbf{W}_{i,j}}{|\mathbf{C}_\ell|} = k - \frac{\phi(C_1, C_2, \dots, C_k)}{2}. \end{aligned}$$

The above equation indicates that the maximization of  $\text{trace}(\mathbf{C}^\top \mathbf{W}\mathbf{C})$  is equivalent to the minimization of  $\phi(C_1, C_2, \dots, C_k)$ , which completes the proof.  $\square$

**Proof of Lemma 5.1.** First, let  $\mathbf{B} = \hat{\mathbf{Z}}\hat{\mathbf{Z}}^\top - \gamma \cdot \frac{\omega\omega^\top}{\omega^\top \mathbf{1}}$ . Consider any cluster  $C_\ell \in \{C_1, C_2, \dots, C_k\}$ . By the definition of  $\mathbf{C}$ , it is easy to verify that

$$\mathbf{C}_{\cdot, \ell}^\top \mathbf{B}\mathbf{C}_{\cdot, \ell} = \sum_{v_i, v_j \in C_\ell} \mathbf{B}_{i,j}.$$

For all the  $k$  clusters, we have

$$\text{trace}(\mathbf{C}^\top \mathbf{B}\mathbf{C}) = \sum_{\ell=1}^k \mathbf{C}_{\cdot, \ell}^\top \mathbf{B}\mathbf{C}_{\cdot, \ell} = \sum_{\ell=1}^k \sum_{v_i, v_j \in C_\ell} \mathbf{B}_{i,j} = \omega^\top \mathbf{1} \cdot \mathbf{Q},$$

which leads to the lemma.  $\square$

**Proof of Theorem 5.2.** Since Eq. (15) is equivalent to  $\mathbf{H} \leftarrow (\hat{\mathbf{Z}}\hat{\mathbf{Z}}^\top - \gamma \cdot \frac{\omega\omega^\top}{\omega^\top \mathbf{1}}) \cdot \mathbf{Q}$ , by Theorem 5.1 in [76], the columns of  $\mathbf{Q}$  are the  $k$ -largest eigenvectors  $\mathbf{Y}$  of  $\hat{\mathbf{Z}}\hat{\mathbf{Z}}^\top - \gamma \cdot \frac{\omega\omega^\top}{\omega^\top \mathbf{1}}$  when  $\mathbf{Q}$  converges.

Next, suppose that matrix  $\tilde{\mathbf{Z}}$  satisfies  $\tilde{\mathbf{Z}}\tilde{\mathbf{Z}}^\top = \hat{\mathbf{Z}}\hat{\mathbf{Z}}^\top - \gamma \cdot \frac{\omega\omega^\top}{\omega^\top \mathbf{1}}$ . According to Lemma 4.1 and Lemma 4.2, the solution  $\mathbf{S}$  to the problem in Eq. (16) is  $\mathbf{S} = \mathbf{U}^{(k)}\mathbf{U}^{(k)\top}$ , where  $\mathbf{U}^{(k)}$  consists of the top- $k$  left singular vectors of  $\tilde{\mathbf{Z}}$ . Similar to the proof of Lemma 4.2, using Theorem C.1 derives that the  $k$ -largest eigenvectors  $\mathbf{Y}$  of  $\tilde{\mathbf{Z}}$  are the top- $k$  left singular vectors of  $\tilde{\mathbf{Z}}$ , namely  $\mathbf{S} = \mathbf{Y}\mathbf{Y}^\top = \mathbf{Q}\mathbf{Q}^\top$ , which completes the proof.  $\square$

**Proof of Lemma A.1.** Let  $\mathbf{\Pi} = \sum_{t=0}^T \frac{(1-\alpha)\alpha^t}{1-\alpha^{T+1}} \hat{\mathbf{P}}^t$ . We prove that  $\mathbf{\Pi}$  is a right stochastic matrix. According to the definition of  $\hat{\mathbf{P}}$  in Section 3.4,  $\forall v_i \in \mathcal{V}$ ,  $\sum_{v_j \in \mathcal{V}} \hat{\mathbf{P}}_{i,j} = 1$  holds, meaning that  $\hat{\mathbf{P}}$  is right stochastic, and thus,  $\hat{\mathbf{P}}^t \forall t \geq 0$  is right stochastic. For any vertex  $v_i \in \mathcal{V}$ ,

$$\begin{aligned} \sum_{v_j \in \mathcal{V}} \mathbf{\Pi}_{i,j} &= \sum_{v_j \in \mathcal{V}} \sum_{t=0}^T \frac{(1-\alpha)\alpha^t}{1-\alpha^{T+1}} \hat{\mathbf{P}}_{i,j}^t = \sum_{t=0}^T \frac{(1-\alpha)\alpha^t}{1-\alpha^{T+1}} \sum_{v_j \in \mathcal{V}} \hat{\mathbf{P}}_{i,j}^t \\ &= \sum_{t=0}^T \frac{(1-\alpha)\alpha^t}{1-\alpha^{T+1}} = 1, \end{aligned}$$

indicating that  $\mathbf{\Pi}$  is right stochastic.

Next, we denote  $\hat{\mathbf{X}}\hat{\mathbf{X}}^\top$  by  $\mathbf{B}$ . We can represent  $\mathbf{Z}\mathbf{Z}^\top$  as  $\mathbf{\Pi}\mathbf{B}\mathbf{\Pi}^\top$ , and hence, for  $v_i \in \mathcal{V}$ ,

$$\begin{aligned} \sum_{v_j \in \mathcal{V}} \mathbf{Z}_i \mathbf{Z}_j^\top &= \sum_{v_j \in \mathcal{V}} \sum_{v_h \in \mathcal{V}} \sum_{v_\ell \in \mathcal{V}} \mathbf{\Pi}_{i,\ell} \cdot \mathbf{B}_{\ell,h} \cdot \mathbf{\Pi}_{j,h} \\ &= \sum_{v_j \in \mathcal{V}} \sum_{v_\ell \in \mathcal{V}} \mathbf{\Pi}_{i,\ell} \sum_{v_h \in \mathcal{V}} \mathbf{B}_{\ell,h} \cdot \mathbf{\Pi}_{j,h} \\ &= \sum_{v_\ell \in \mathcal{V}} \mathbf{\Pi}_{i,\ell} \sum_{v_h \in \mathcal{V}} \mathbf{B}_{\ell,h} \sum_{v_j \in \mathcal{V}} \mathbf{\Pi}_{j,h}. \end{aligned}$$

Then, by the definitions of  $\beta_\ell$  and  $\pi_\ell$ ,

$$\begin{aligned} \sum_{v_\ell \in \mathcal{V}} \mathbf{\Pi}_{i,\ell} \sum_{v_h \in \mathcal{V}} \mathbf{B}_{\ell,h} \sum_{v_j \in \mathcal{V}} \mathbf{\Pi}_{j,h} &\leq \max_{v_\ell \in \mathcal{V}} \beta_\ell \cdot \pi_\ell \cdot \sum_{v_\ell \in \mathcal{V}} \mathbf{\Pi}_{i,\ell} \\ \sum_{v_\ell \in \mathcal{V}} \mathbf{\Pi}_{i,\ell} \sum_{v_h \in \mathcal{V}} \mathbf{B}_{\ell,h} \sum_{v_j \in \mathcal{V}} \mathbf{\Pi}_{j,h} &\geq \min_{v_\ell \in \mathcal{V}} \beta_\ell \cdot \pi_\ell \cdot \sum_{v_\ell \in \mathcal{V}} \mathbf{\Pi}_{i,\ell}. \end{aligned}$$

Since  $\mathbf{\Pi}$  is a right stochastic matrix, we can get

$$\min_{v_\ell \in \mathcal{V}} \beta_\ell \cdot \pi_\ell \leq \sum_{v_j \in \mathcal{V}} \mathbf{Z}_i \mathbf{Z}_j^\top \leq \max_{v_\ell \in \mathcal{V}} \beta_\ell \cdot \pi_\ell,$$

which finishes the proof.  $\square$

**Proof of Lemma A.2.** Let  $F$  be  $XX^\top$  and hence  $F_{i,j} = X_i \cdot X_j^\top \forall v_i, v_j \in \mathcal{V}$ . By the definition of  $\hat{X}$  in Section 3.4,

$$\hat{X}_i \cdot \hat{X}_j^\top = \frac{F_{i,j}}{\sqrt{\sum_{v_\ell \in \mathcal{V}} F_{i,\ell}} \sqrt{\sum_{v_\ell \in \mathcal{V}} F_{j,\ell}}}.$$

Next, we can derive

$$\begin{aligned} \frac{1}{n^2} \sum_{v_i, v_j \in \mathcal{V}} \hat{X}_i \cdot \hat{X}_j^\top &= \frac{1}{n^2} \sum_{v_i, v_j \in \mathcal{V}} \frac{F_{i,j}}{\sqrt{\sum_{v_\ell \in \mathcal{V}} F_{i,\ell}} \sqrt{\sum_{v_\ell \in \mathcal{V}} F_{j,\ell}}} \\ &= \frac{1}{n^2} \sum_{v_i, v_j \in \mathcal{V}} \sqrt{\frac{F_{i,j}}{\sum_{v_\ell \in \mathcal{V}} F_{i,\ell}}} \cdot \sqrt{\frac{F_{i,j}}{\sum_{v_\ell \in \mathcal{V}} F_{j,\ell}}} \end{aligned}$$

Using Cauchy–Schwarz inequality, we have

$$\begin{aligned} &\frac{1}{n^2} \sum_{v_i, v_j \in \mathcal{V}} \sqrt{\frac{F_{i,j}}{\sum_{v_\ell \in \mathcal{V}} F_{i,\ell}}} \cdot \sqrt{\frac{F_{i,j}}{\sum_{v_\ell \in \mathcal{V}} F_{j,\ell}}} \\ &\leq \frac{1}{n^2} \sqrt{\sum_{v_i, v_j \in \mathcal{V}} \frac{F_{i,j}}{\sum_{v_\ell \in \mathcal{V}} F_{i,\ell}} \cdot \sum_{v_i, v_j \in \mathcal{V}} \frac{F_{i,j}}{\sum_{v_\ell \in \mathcal{V}} F_{j,\ell}}} \\ &= \frac{1}{n^2} \sqrt{\sum_{v_i \in \mathcal{V}} \frac{\sum_{v_j \in \mathcal{V}} F_{i,j}}{\sum_{v_\ell \in \mathcal{V}} F_{i,\ell}} \cdot \sum_{v_j \in \mathcal{V}} \frac{\sum_{v_i \in \mathcal{V}} F_{i,j}}{\sum_{v_\ell \in \mathcal{V}} F_{j,\ell}}} = \frac{1}{n^2} \sqrt{n \cdot n} = \frac{1}{n}. \end{aligned}$$

The lemma is proved.  $\square$

**Proof of Lemma A.3.** First, we denote  $\sum_{t=0}^T \frac{(1-\alpha)\alpha^t}{1-\alpha^{T+1}} \hat{P}^t$  by  $\Pi$ . According to the definition of  $\hat{P}$  in Section 3.4, we can deduce that  $\hat{P} = \hat{D}^{-1} \hat{A}$ , where  $\hat{D}$  is a diagonal matrix wherein each entry  $\hat{D}_{h,h}$  equals  $\hat{d}(v_h)$ . Accordingly,  $\Pi \hat{D}^{-1}$  is a symmetric matrix. This leads to  $\frac{\Pi_{h,\ell}}{\hat{d}(v_\ell)} = \frac{\Pi_{\ell,h}}{\hat{d}(v_h)}$ . Recall that  $\Pi$  is a right stochastic matrix (see the proof of Lemma A.1), which implies  $\sum_{v_h \in \mathcal{V}} \Pi_{h,\ell} \cdot \frac{\hat{d}(v_h)}{\hat{d}(v_\ell)} = 1$ . Consequently,

$$\frac{\hat{d}(v_\ell)}{\max_{v_h \in \mathcal{N}_{v_\ell} \cap \{v_\ell\}} \hat{d}(v_h)} \leq \sum_{v_h \in \mathcal{V}} \Pi_{h,\ell} \leq \frac{\hat{d}(v_\ell)}{\min_{v_h \in \mathcal{N}_{v_\ell} \cap \{v_\ell\}} \hat{d}(v_h)}.$$

The lemma naturally follows.  $\square$